Turun yliopisto
University of Turku

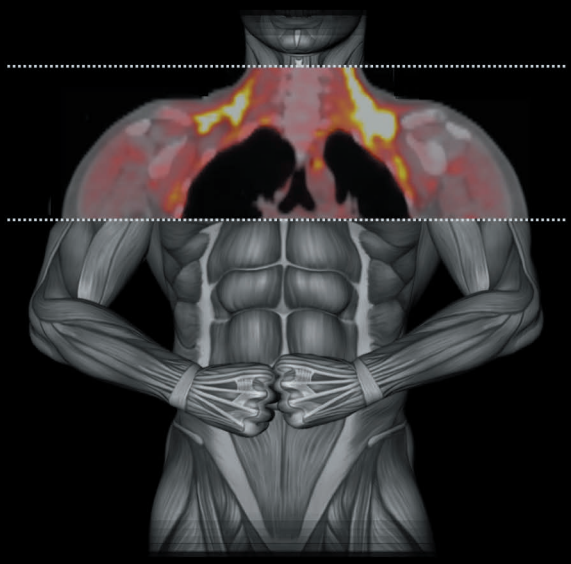

OXIDATIVE METABOLISM AND NON-INVASIVE CHARACTERISATION OF BROWN ADIPOSE TISSUE IN ADULT HUMANS

Mueez u Din

TURUN YLIOPISTON JULKAISUJA - ANNALES UNIVERSITATIS TURKUENSIS
Sarja - ser. D osa - tom. 1348 | Medica - Odontologica | Turku 2018

Turun yliopisto
University of Turku

OXIDATIVE METABOLISM AND NON-INVASIVE CHARACTERISATION OF BROWN ADIPOSE TISSUE IN ADULT HUMANS

Mueez u Din

TURUN YLIOPISTON JULKAISUJA – ANNALES UNIVERSITATIS TURKUENSIS
Sarja - ser. D osa - tom. 1348 | Medica - Odontologica | Turku 2018

University of Turku

Faculty of Medicine
Department of Clinical Physiology and Isotope Medicine
Doctoral Programme in Clinical Research
Turku PET Centre
Turku University Hospital

Supervised by

Docent Kirsi A. Virtanen, MD, PhD
Turku PET Centre, University of Turku
Turku, Finland

Professor Pirjo Nuutila, MD, PhD
Turku PET Centre, University of Turku
Department of Endocrinology,
Turku University Hospital
Turku, Finland

Reviewed by

Professor Abdul G. Dulloo
Department of Medicine, University of Fribourg
Fribourg, Switzerland

Professor (Emeritus) Esa Hohtola
Department of Ecology and Genetics,
University of Oulu
Oulu, Finland

Opponent

Professor Atso Raasmaja
Division of Pharmacology and Pharmacotherapy
Faculty of Pharmacy, University of Helsinki
Helsinki, Finland

Cover Image by Mueez u Din

ISBN 978-951-29-7219-7 (PRINT)
ISBN 978-951-29-7220-3 (PDF)
ISSN 0355-9483 (Print)
ISSN 2343-3213 (Online)
Painosalama Oy – Turku, Finland 2018

To those who believed
in me and stood by
my side

ABSTRACT

Mueez u Din

Oxidative metabolism and non-invasive characterisation of brown adipose tissue in adult humans

University of Turku, Faculty of Medicine, Department of Clinical Physiology and Isotope Medicine, Doctoral Programme in Clinical Research, and Turku PET Centre

Annales Universitatis Turkuensis, Turku, Finland, 2018

In adult humans, brown adipose tissue (BAT) has been found to be metabolically active. However, the physiological relevance of BAT in adult humans is still imprecise and largely speculative. The study of oxidative metabolism of BAT during different physiological states can unravel the significance of BAT in whole-body energy metabolism; and meanwhile there is also a need to improve the characterisation of BAT using the existing non-invasive medical imaging methods.

The aim of the doctoral work was to evaluate whether the oxygen consumption of BAT in adult humans, measured using positron emission tomography, is influenced by cold stress, and with the ingestion of a mixed meal. Cold-induced and meal-induced whole-body thermogenesis was also studied. Additionally, the utility of a non-invasive medical imaging method of x-ray computed tomography to provide metabolic information related to BAT was investigated.

The results showed that cold stress, as well as ingestion of a mixed meal, increases the oxygen consumption of BAT. However, the overall capacity of BAT to contribute to cold-induced and meal-induced whole-body thermogenesis is limited. The x-ray computed tomography derived metrics of BAT has the potential to give an insight into underlying tissue composition and substrate metabolism, and this characteristic can be exploited to make a distinction between white adipose tissue and BAT.

Keywords: Human brown adipose tissue, oxidative metabolism, PET-CT imaging

TIIVISTELMÄ

Mueez u Din

Ruskean rasvakudoksen oksidatiivinen aineenvaihdunta ja kajoamaton karakterisointi aikuisilla ihmisillä

Turun yliopisto, Lääketieteellinen tiedekunta, Kliininen fysiologia, isotooppilääketiede ja PET, Turun kliininen tohtoriohjelma (TKT), Valtakunnallinen PET-keskus

Annales Universitatis Turkuensis, Turku, Finland, 2018

Aikuisilla ihmisillä ruskean rasvakudoksen (BAT) on todettu olevan toiminnallisesti aktiivinen. Ruskean rasvan fysiologinen merkitys on kuitenkin vielä epäselvä ja perustuu suurelta osin oletuksiin. Ruskean rasvan oksidatiivisen aineenvaihdunnan tutkiminen eri fysiologisissa tilanteissa voi selventää ruskean rasvan osuutta koko kehon energia-aineenvaihdunnassa. Samanaikaisesti on tarve kehittää entistä parempia menetelmiä ja kehittää olemassa olevia kajoamattomia lääketieteellisiä kuvantamismenetelmiä ruskean rasvan tarkempaan tunnistamiseen ja karakterisointiin.

Väitöskirjatyön tavoitteena oli selvittää, miten ruskean rasvan hapenkulutus eli oksidatiivinen aineenvaihdunta, positroniemissiotomografialla (PET) mitattuna, muuttuu kylmäaltistuksen vaikutuksesta ja toisaalta yksittäisen aterian syömisen jälkeen. Koko kehon energiankulutus mitattiin samoissa tilanteissa epäsuoraa kalorimetriaa käyttäen. Tämän lisäksi selvitettiin kajoamattoman lääketieteellisen tietokonetomografian (TT) käytettävyyttä ruskean rasvan aineenvaihdunnan tutkimuksessa.

Kylmäaltistus ja aterian syöminen lisäsivät molemmat ruskean rasvakudoksen hapenkulutusta. Koko kehon tasolla ruskean rasvan osuus kylmästimuloidusta ja ruokailun aiheuttamasta lämmöntuotannosta on kuitenkin rajallinen ja kudoksen pieni koko huomioiden pieni. Tietokonetomografian avulla mitattujen tunnuslukujen avulla on mahdollista saada käsitys ruskea rasvakudoksen koostumuksesta ja aineenvaihdunnasta, ja näitä ominaisuuksia voidaankin hyödyntää erottamaan ruskea rasvakudos valkoisesta rasvakudoksesta.

Avainsanat: Ruskea rasvakudos, oksidatiivinen aineenvaihdunta, metabolia, PET, TT, PET-TT-kuvantaminen

TABLE OF CONTENTS

ABBREVIATIONS

^{1}H-MRS	^{1}H-magnetic resonance spectroscopy
[^{18}F]FDG	[^{18}F]2-fluoro-2-deoxy-D-glucose
[^{18}F]FTHA	14(R,S)-[^{18}F]fluoro-6-thia-heptadecanoic acid
AC	adenylyl cyclase
Acetyl-CoA	acetyl co-enzyme A
ATGL	adipose triglyceride lipase
ATP	adenosine triphosphate
BAT	brown adipose tissue
BMI	body mass index
CAC	citric acid cycle
cAMP	3',5'-cyclic adenosine monophosphate
CD36	cluster of differentiation 36
CIT	cold induced thermogenesis
CT	x-ray computed tomography
DEE	daily energy expenditure
DIT	diet induced thermogenesis
ECG	electrocardiography
EE	energy expenditure
En1	engrailed-1
FATP	fatty acid transport proteins
FFA	free fatty acid / non-esterified fatty acid
FGF	fibroblast growth factor
FOV	field of view
GCP	good clinical practice
G_s protein	stimulatory G protein
GLUT-1	glucose transporter protien-1
GLUT-4	glucose transporter protien-4
GMP	good medical practice
HDL	high-density lipoprotein
HSL	hormone-sensitive lipase
HU	Hounsfield unit
LDL	low-density lipoprotein
LPL	lipoprotein lipase
MIT	meal induced thermogenesis
MRI	magnetic resonance imaging

MRO_2	metabolic rate of oxygen consumption
MRS	magnetic resonance spectroscopy
M-value	whole-body insulin sensitivity
Myf5	myogenic factor 5
NE	norepinephrine
NEFA	non-esterified fatty acid / free fatty acid
NP	natriuretic peptides
NPR	natriuretic peptides receptors
NSA	number of signal averages
NST	non-shivering thermogenesis
OGTT	oral glucose tolerance test
OSEM	ordered subset expectation maximization
PET	positron emission tomography
PKA	protein kinase A
PRESS	pointed- resolved spectroscopy
ROC	receiver-operating characteristic
RPKM	reads per 1kb transcript length per million mapped reads
RQ	respiratory quotient
RT	room temperature
SNS	sympathetic nervous system
SUV	standardized uptake value
T3	triiodothyronine
T4	thyroxine
TAC	time activity curve
TAG	triacylglycerol
TE	repetition time
TR	echo time
TRG5	G-protein coupled bile receptors
TSH	thyroid-stimulating hormone
UCP-1	uncoupling protein -1
V_A	arterial blood volume
vO_2	rate of oxygen consumption (whole-body)
vCO_2	rate of carbon dioxide production (whole-body)
VOI	volumes of interest
WAT	white adipose tissue

LIST OF ORIGINAL PUBLICATIONS

This thesis is based on the following original publications, which are referred to in the text by the Roman numerals I – III:

I. U Din M., Raiko J., Saari T., Kudomi N., Tolvanen T., Oikonen V., Teuho J., Sipila H.T., Savisto N., Parkkola R., Nuutila P., and Virtanen K.A. 2016 Human brown adipose tissue [^{15}O]O_2 PET imaging in the presence and absence of cold stimulus. *Eur J Nucl Med Mol Imaging* 43, 1878-1886

II. U Din M.*, Saari T.*, Raiko J., Kudomi N., Maurer F.S., Lahesmaa M., Fromme T., Amri E.Z., Klingenspor M., Solin O., Nuutila P., and Virtanen K.A. 2018 Postprandial metabolic response of human brown fat and meal induced thermogenesis. (submitted)

III. U Din M., Raiko J., Saari T., Saunavaara V., Kudomi N., Solin O., Parkkola R., Nuutila P., and Virtanen K.A. 2017 Human brown fat radiodensity indicates underlying tissue composition and systemic metabolic health. *J Clin Endocrinol Metab* 102 (7), 2258-2267

* Equal contributor

1 INTRODUCTION

In the present world we live in, among the many other problems we face related to human health, one of great concern is obesity. Obesity is characterised by the accumulation of excess energy in the form of fat in the body. These excess fat deposits interfere with the other normal physiological mechanisms of the body and lead toward the development of additional health complications including diabetes and problems of the cardiovascular system. In the clinical guidelines, the method of combating obesity is not only the modification of energy intake, but also increasing the energy consumption by the body. Physical exercise is one of the suggested methods to increase this energy expenditure. In a quest for other methods to increase energy expenditure, it has been noticed that humans have an increase in energy expenditure under cold stress. Simultaneously, it was noticed that in mammals, including human infants, the brown adipose tissue (BAT) is a distinct type of adipose tissue, which is active during cold stress and it burns the energy in the form of heat. This finding led scientists to speculate that brown adipose tissue has a tremendous energy dissipating potential. However, at that time, this type of adipose tissue was thought to be not present in adult humans. The recent technological advances in medical imaging made it possible to reveal that in fact adult humans also possess BAT. This intrigued the scientific community whether the tremendous energy dissipating potential of BAT can be channelled to increase the energy expenditure of the body, and thus it could be one of the viable options for the treatment of obesity.

Since the Turku PET centre has a strong expertise in the field of medical imaging, these intriguing questions posited by the scientific community could be answered utilising various medical imaging techniques. Therefore, this thesis work was executed to examine the physiological significance of human BAT in energy metabolism. The aim of this work was to answer the existing questions of the scientific community, as well as to help lead the human race in the right direction as regards finding adequate approaches to combating obesity.

Thus, in this thesis the oxidative metabolism of human brown adipose tissue has been evaluated with $[^{15}O]O_2$ PET imaging. Furthermore, the potential role of BAT in whole-body energy metabolism, particularly cold-induced and meal-induced thermogenesis, has been evaluated. The utility of the x-ray computed tomography to provide the metabolic information related to BAT, in addition to the existing role of anatomical localisation, has also been explored.

2 REVIEW OF LITERATURE

2.1 Adipose tissue

2.1.1 White adipose tissue

The adipose tissue where the lipids are accumulated in the form of a unilocular entity, i.e. a large lipid droplet, inside the adipocytes is known as white adipose tissue [WAT, (Cinti, 2006)]. The prominent role of WAT in the human body is the storage of excess energy in the form of lipids (Gesta et al., 2007).

The depots of WAT are widely distributed in the human body; though the main locations are under the skin (subcutaneous WAT) and inside the abdominal cavity (intra-abdominal WAT) (Gesta et al., 2007). The main location for the presence of subcutaneous WAT in an adult human is the abdominal and gluteal region (Bjorndal et al., 2011). The intra-abdominal WAT surrounds the abdominal organs, and based on the proximity to the peritoneal cavity it is further interchangeably classified as visceral, omental, mesenteric, intraperitoneal and retroperitoneal adipose tissue (Bjorndal et al., 2011; Gesta et al., 2007). In addition to these locations, the WAT can be found in smaller depots in retro-orbital space (Ilankovan and Soames, 1995), bone marrow (Zakaria and Shafrir, 1967), and in the regions around blood vessels (Schlett et al., 2009), mediastinum (Sanei et al., 2015), bone joints (Clockaerts et al., 2010), and heart (Iacobellis et al., 2005).

2.1.2 Brown adipose tissue

The adipose tissue with the unique capacity to generate heat by the consumption of substrates is commonly known as brown adipose tissue (BAT). This adipose tissue is labelled as ‘brown’ due to its characteristic brownish macroscopic appearance (Cinti, 2005). The brownish colour of brown adipocytes is due to the dissimilar cellular composition compared to white adipocytes. The brown adipocytes characteristically possess several small multilocular lipid droplets (Cinti, 2006), and it is densely packed with mitochondria (Lindberg et al., 1967). The brown fat depots are highly vascularised (Hausberger and Widelitz, 1963)

and abundantly innervated by sympathetic nerve efferent fibres (Bartness et al., 2010). The presence of small lipid droplets, instead of a single large droplet, aids the brown adipocytes to increase the surface-to-volume ratio of the stored lipids. This structural property facilitates extra sites in the brown adipocytes to have for lipolysis reactions, thus making fatty acids readily available in larger quantities for respiratory chain reactions (Cinti, 2012). The histology as well as diagrammatic representation of brown and white adipocyte are shown in Figure 1.

The ability of brown adipocytes to produce heat comes from the presence of a large number of mitochondria together with a high expression of uncoupling protein -1 [UCP-1, (Lean and James, 1983)]. The brown adipocytes express low levels of ATP-synthase (Kramarova et al., 2007) which is usually used to produce adenosine triphosphate (ATP) by utilising the proton gradient across the mitochondrial inner membrane in the cellular respiration. In the mitochondria of brown adipocytes the presence of high levels UCP-1, instead of ATP-synthase, allows the diminishing of the proton gradient by uncoupling cellular respiration without the production of ATP, and dissipating energy in the form of heat (Cannon and Nedergaard, 2004).

In human neonates and infants, BAT has been reported to be anatomically present in intrascapular, supraclavicular, axillary, neck and suprarenal areas (Aherne and Hull, 1966). Human neonates, compared to adults, have higher body surface-to-volume ratio and additionally less muscle mass; therefore, the maintenance of the body temperature is challenging and requires non-shivering means of heat generation. The brown fat in neonates constitutes approximately 5% of the body weight. As the neonates become older much of the BAT depots disappear, while some remain until adult life (Heaton, 1972). In human adults, the major sites of the presence of BAT depots include the fat depots in between neck muscles, supraclavicular fat depots, axilla, lungs hilum, around cardiac muscles, supra- and peri-renal and adrenals, around blood vessels (e.g. around the aorta) (Heaton, 1972) and along the vertebral column in the form of small fat depots (Sacks and Symonds, 2013) (Figure 2). The reported mass of brown fat in adult humans, from *in vivo* imaging studies, is highly variable; although the amount usually ranges from 0.02 grams to 300 grams (Cypess et al., 2009; Gerngroß et al., 2017; van Marken Lichtenbelt et al., 2009; Muzik et al., 2012; Orava et al., 2011) which constitutes less than 0.5 percent (%) of an average adult human body mass (75 kg).

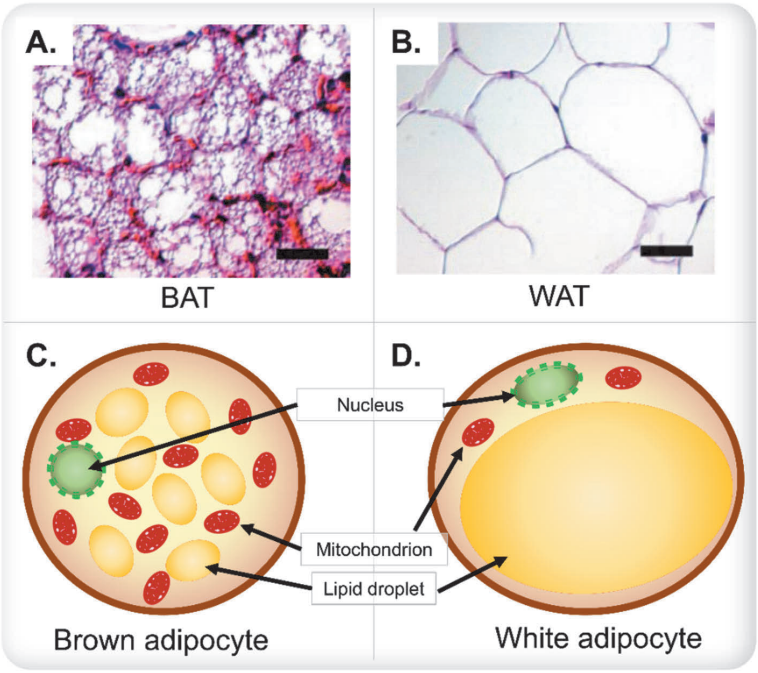

Figure 1. The histology of BAT and WAT, and a diagrammatic representation of brown and white adipocytes.
A. The histological appearance of a human BAT sample from a supraclavicular depot, showing multilocular intracellular lipid droplets. **B.** The histological appearance of a human WAT sample. **C.** A diagrammatic representation of a brown adipocyte with several small intracellular lipid droplets and a high mitochondrial density. **D.** A diagrammatic representation of a white adipocyte with a single large lipid droplet, which pushes other cellular structures to the sides. (**A** & **B** are adapted from Virtanen et al., 2009)

2.1.3 Beige/brite adipose tissue

Earlier, it was considered that all UCP-1 positive thermogenic adipocytes can be categorised as brown adipocytes. However, later evidence suggested that there are two types of UCP-1 positive thermogenic adipocytes which arise from distinct developmental lineages (Wu et al., 2012). The 'classical brown adipocytes' arise from engrailed-1 (*En1*) expressing cells of the central dermomyotome (Atit et al., 2006), and myogenic factor 5 (*Myf5*) positive progenitor cells (Seale et al., 2008); while, 'brown-like' adipocytes originate

from *Myf5* negative progenitor cells (Ishibashi and Seale, 2010; Seale et al., 2008). These brown-like adipocytes have been interchangeably termed as 'brite' (Petrovic et al., 2010), 'beige' (Ishibashi and Seale, 2010) or 'recruitable brown' (Enerbäck, 2009) due to their occurrence within white adipose tissue histologically in the form of clusters of small islands (Cypess and Kahn, 2010), and reversible white-to-brown transdifferentiation (Cinti, 2009).

The classical brown adipocytes and beige/brite adipocytes express unique markers of gene expressions reflecting their developmental origin (Walden et al., 2012). The evidence from genetic analysis suggests that in adult humans the brown fat depots (e.g. supraclavicular fat depots) mainly consist of beige/brite adipocytes (Sharp et al., 2012; Wu et al., 2012), while the classical brown adipocytes are usually found in rodents and human infants (e.g. interscapular fat depots) (Lidell et al., 2013). However, one study also shows a contrasting finding that human supraclavicular depot express markers of both classical-brown and beige adipose tissue markers (Jespersen et al., 2013). The total amount of UCP-1 protein in beige/brite adipocytes has been reported to be approximately 10% of the classical brown adipocytes; therefore, the overall UCP-1-dependent thermogenic capacity of beige/brite adipocytes may be lower than classical brown adipocytes (Nedergaard and Cannon, 2013).

Since BAT is the popular term used in the academic community as well as scientific literature for both brite/beige/recruitable-BAT and classical-BAT, this thesis terms both 'brite/beige/recruitable-BAT' and 'classical-BAT' as, BAT or brown fat.

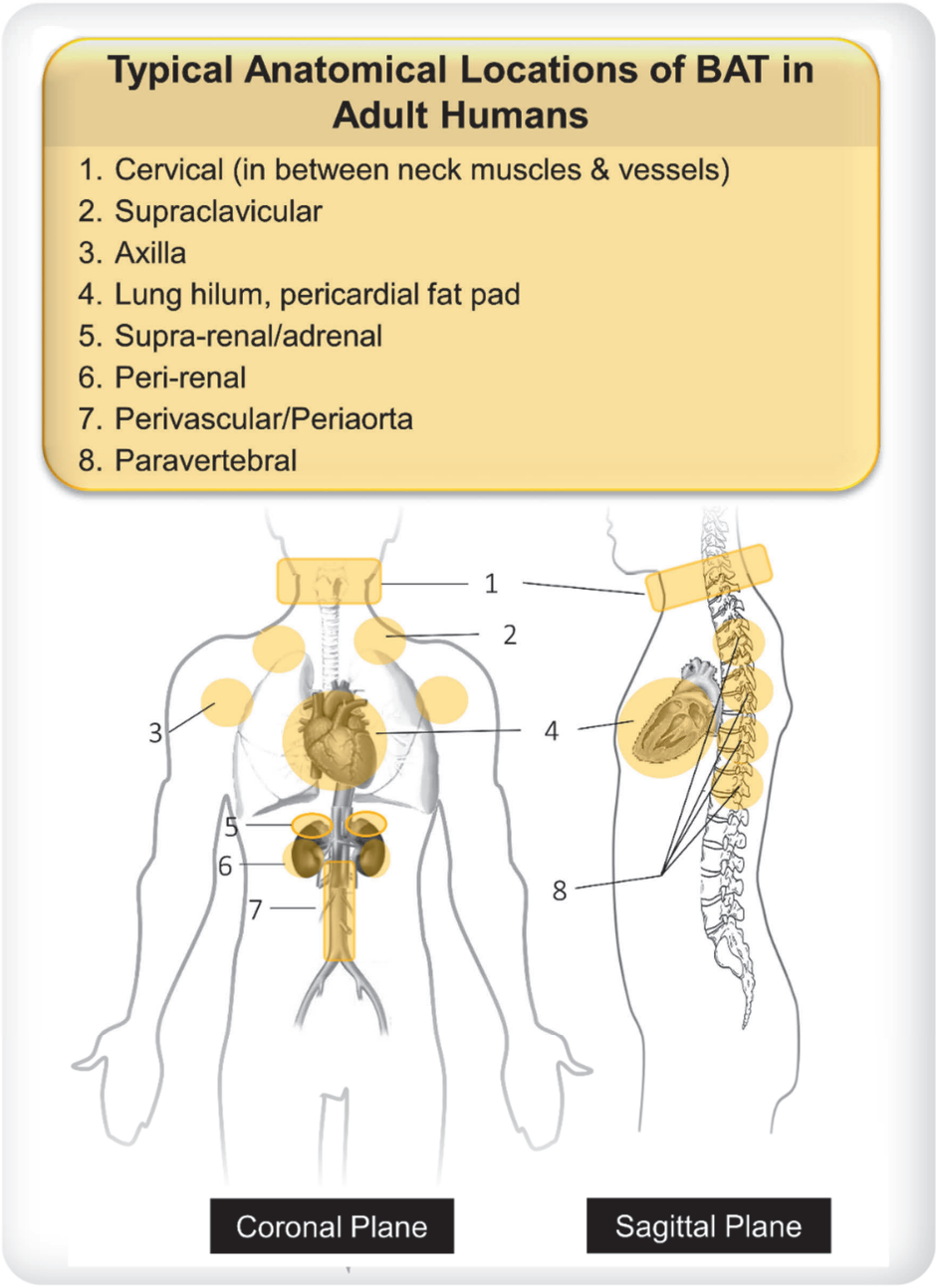

Figure 2. The typical anatomical locations for the presence of BAT in adult humans based on imaging and human autopsy findings (Heaton, 1972; Sacks and Symonds, 2013).

2.2 Oxidative metabolism of brown adipose tissue

2.2.1 Thermogenesis in brown adipose tissue

In general, cellular respiration is a process in which oxygen reacts with substrate molecules (e.g. glucose, fatty acids, and ketone bodies) to produce water, carbon dioxide and ATP. Specifically, the cellular respiration reaction within a mitochondrion mainly consist of citric acid cycle (CAC) (Krebs, 1948) and oxidative phosphorylation (Mitchell, 1966; Slater, 1953). In the CAC, the acetyl co-enzyme A (acetyl-CoA), which can be derived from carbohydrates, fats or proteins, is oxidized to produce ATP. While in the oxidative phosphorylation, the molecular oxygen is directly used to produce ATP from the activity of ATP-synthase (via the process called chemiosmosis) due to the presence of a proton gradient formed by an electron transport chain (Mitchell and Moyle, 1967). The oxygen for these cellular respiration reactions in humans is supplied via circulation; while in circulation the oxygen comes from the whole-body respiration via the respiratory system.

However, the cellular respiration in brown adipocytes is unique. It is exclusive in a way that in active brown fat mitochondria, the energy liberated in cellular respiration is released as heat instead of being used for ATP-synthesis. This direct thermogenic ability of BAT is due to the presence of UCP-1 (Jezek and Garlid, 1998); which is a BAT-specific protein located in the inner membrane of the mitochondria in a brown adipocyte (Aquila et al., 1985; Bouillaud et al., 1986). In addition to the presence of UCP-1, the brown adipocytes have low levels of ATP-synthase (Kramarova et al., 2007). The UCP-1 allows a proton leak across the inner mitochondrial membrane, formed by the electron transport chain, without the production of ATP. This release of the proton gradient, due to UCP-1, comes along with the generation of heat (Crichton et al., 2017; Klingenspor, 2003). This UCP-1 mediated conductance of protons is activated by free fatty acids (Fedorenko et al., 2012), and it is inhibited by purine nucleotides (Divakaruni et al., 2012; Shabalina et al., 2004). The UCP-1 mediated thermogenesis in brown adipocyte has been diagrammatically illustrated in Figure 3.

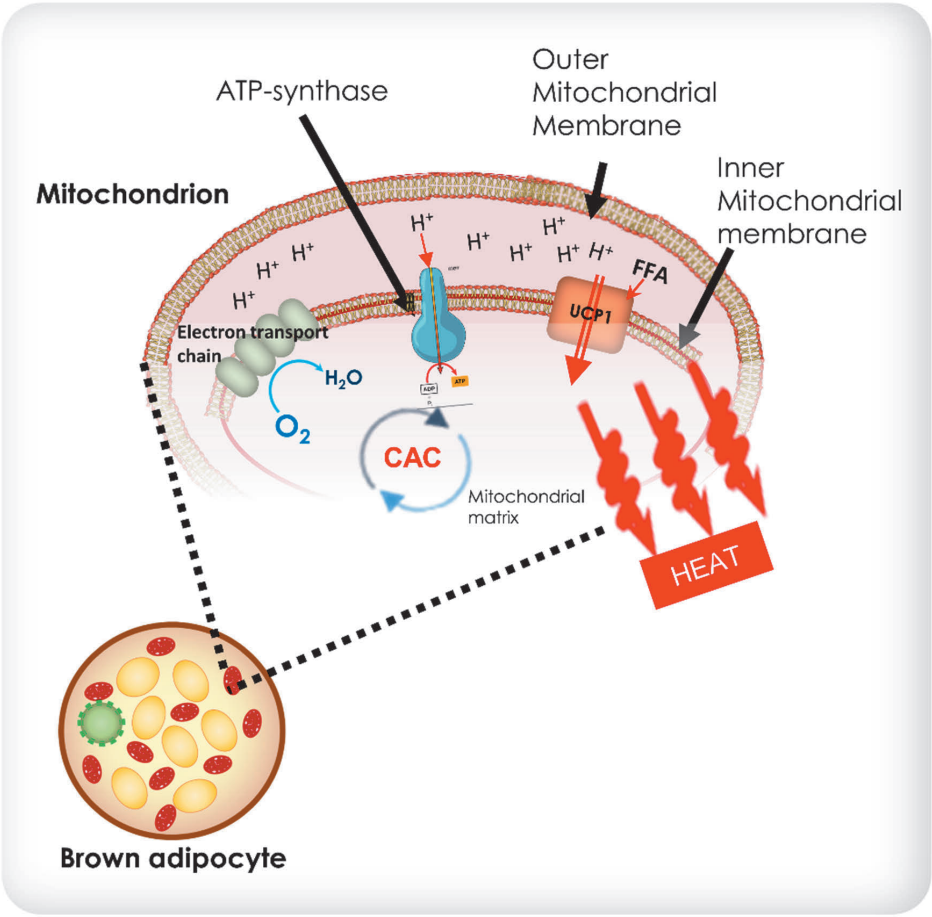

Figure 3. A diagrammatic illustration of the UCP-1 mediated cellular respiration which leads to the production of heat instead of ATP in a brown adipocyte (references are provided in the main text).

Hence, the energy production by the cells is directly dependent on the cellular respiration where some of the energy is dissipated as heat and some trapped in the high energy molecules, ATPs. While the cellular respiration reactions are dependent on the oxidation of the substrates, the measurement of the amount of oxygen consumption provides a direct estimate of the total amount of produced energy. The method of measuring the whole-body energy expenditure by indirect calorimetery is dependent on the same principle where the oxygen consumption and carbon-dioxide production of the entire body is measured based on the amount of inspired O_2 and expired CO_2 via the respiratory system (Ferrannini, 1988).

The presence of several mitochondria in the brown adipocytes increases the overall capacity of BAT for cellular respiration, as well as heat production. In the adult human body, the eccentric distribution of brown fat (Figure 2) is likely to be of thermogenic importance; however, the currently reported functional relevance of the location of human BAT is largely speculative, and/or based on rodent studies. The significance of perivascular brown fat is likely to act as an active metabolic heater for the intervascular flowing blood to and from cooler periphery (Smith, 1964). The cervical BAT has been suggested to maintain the temperature of the extracranial arterial blood owing to the close proximity to common carotid and vertebral arteries (Sacks and Symonds, 2013). BAT located in the axillary and supraclavicular region most likely warms the venous blood from the subclavian and jugular veins (Sacks and Symonds, 2013), and thus possibly protects against cardiac arrhythmias since myocardium is sensitive to lower coronary blood temperatures (Mattu et al., 2002). Likewise, the closer proximity of supraclavicular BAT to the brachial plexus, and paravertebral BAT to the spinal cord, possibly provide protection against hypothermia for the optimal function and nerve conduction of the central and autonomic nervous system (Sacks and Symonds, 2013).

2.2.2 Stimulators of brown adipose tissue

BAT is a tissue with thermogenic ability and, as can be expected, BAT has been found to be active during cold stress. The metabolic stimulation of brown adipocytes during a cold stimulus is via norepinephrine (NE)-dependent signal transduction pathway due to the activation of the sympathetic nervous system (SNS) (Young et al., 1982). On the cell membrane of the brown adipocytes, the NE acts via the G protein (G_s)-coupled β_3-adrenergic receptors to activate adenylyl cyclase (AC) (Bourová et al., 2000). The AC is an enzyme which has the function of converting ATP into 3'-5'-cyclic adenosine monophosphate (cAMP) (Patel et al., 2001). The cAMP further binds to activate the enzyme protein kinase A (PKA) (McKnight et al., 1998). PKA has the role of phosphorylating several proteins, including perilipin (Chaudhry and Granneman, 1999) and hormone-sensitive lipase (HSL) (Krintel et al., 2009). Perilipin, being the protein that coats the lipid droplets in the adipose tissue, changes the conformation due to the activity of PKA and exposes the stored lipid to the activity of HSL. The HSL, subsequent to the action of adipose triglyceride lipase

(ATGL) (Zimmermann et al., 2004), hydrolyses the stored triglycerides to release free fatty acids (FFA). The produced FFA, inside the cytosol and presumably bound to the fatty acid binding proteins (Vergnes et al., 2011), move inside the mitochondria. In the case of short-chain FFAs, this movement across the mitochondrial membranes occurs via diffusion, and in case of long-chain FFA it occurs by the carnitine shuttle (Borum, 1991). These FFA further undergo the process of degradation, β-oxidation, to produce acetyl-CoA, which is subsequently oxidized in cellular thermogenic respiration (section 2.2.1). Additionally, these FFA also activate UCP-1 in the inner membrane of the mitochondria to shunt the proton gradient to produce heat. The schematic illustration of the NE-dependent signal transduction pathway is illustrated in Figure 4.

Insulin has been shown to induce the uptake of glucose in BAT (Ebner et al., 1987; Inokuma et al., 2005; Orava et al., 2011); however the direct influence of insulin on BAT thermogenesis is unclear. Insulin promotes the gene expression of the glucose transporter protien-4 (GLUT-4) in the brown adipocytes, and the increased uptake of glucose due to insulin is GLUT-4 mediated (Omatsu-Kanbe et al., 1996). The glucose transporter protien-1 (GLUT-1) is also present on the cell surface of brown adipocytes, although it is not likely that it influences the insulin-mediated glucose uptake in BAT (Konrad et al., 2002). In addition to the effect of insulin on glucose metabolism, the increased insulin activity also influences fatty acids metabolism. Insulin restricts the activity of the HSL (Nilsson et al., 1980) thus supressing the lipolysis in the adipocytes. Simultaneously, insulin promotes the activity of lipoprotein lipase (LPL) in BAT (Carneheim and Alexson, 1989), which aids in the uptake of circulatory FFA into the brown adipocytes. The fate of these FFAs taken up in BAT following insulin activity is currently unknown. Additionally, it has also been shown that insulin potentially also inhibits the activity of the warm-sensitive neurons present in the hypothalamus, and thus insulin can enhance the thermogenic activity of BAT via the central nervous system (Labbé et al., 2015; Sanchez-Alavez et al., 2010).

A few studies have also identified agents which act together with the SNS pathway or independently to stimulate BAT metabolism (Kooijman et al., 2015; Villarroya and Vidal-Puig, 2013). For example, it has been reported that the bile acids secreted after the consumption of a meal can induce the thermogenic activity in brown adipocytes. The bile acids are thought to activate G-protein

coupled bile receptors (TRG5) which are abundant on the surface of brown adipocytes (Broeders et al., 2015; Watanabe et al., 2006). Additionally, fibroblast growth factor-21 (FGF-21) also interacts with the FGF receptors on the brown adipocytes and they have been shown to stimulate glucose oxidation and thermogenic mechanism in BAT (Fisher et al., 2012; Hanssen et al., 2015a; Hondares et al., 2010). Moreover, the cardiac natriuretic peptides (NP), both atrial and ventricular natriuretic peptides, have been shown to interact with the natriuretic peptides receptors (NPR) on the brown adipocytes surface to induce thermogenic stimulation. The stimulation of NPR eventually converges to the standard brown adipocyte thermogenic transduction pathway (Bordicchia et al., 2012; Collins and Bordicchia, 2013; Wu et al., 2017).

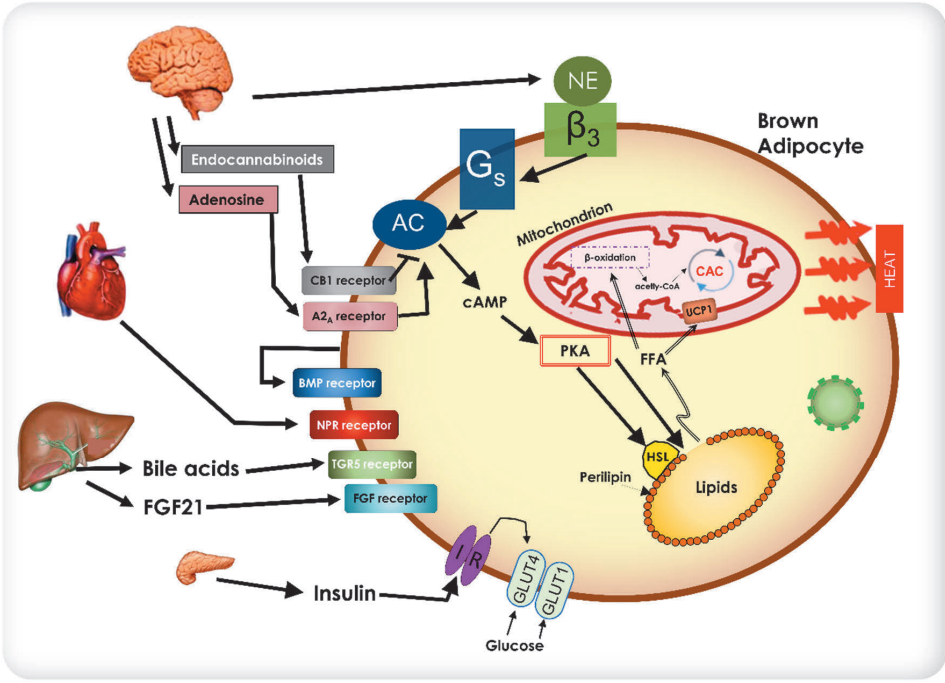

Figure 4. A schematic illustration of the norepinephrine-dependent signal transduction pathway for the thermogenic activation of a brown adipocyte. Additionally, the other stimulators which may act along the SNS pathway or independently to activate BAT thermogenesis have also been highlighted (references are provided in the main text).

2.2.3 Substrate utilization by brown adipose tissue

Free fatty acids (non-esterified fatty acids) have been suggested to be a major substrate for brown adipocytes. These free fatty acids can be obtained directly from the intracellular triglyceride stores after lipolysis, and as well from the blood circulation. Glucose has been considered a minor substrate for BAT. However, the indication of free fatty acids being the major and glucose being the minor substrate of BAT comes from rodent studies (Ma and Foster, 1986), and in humans this phenomena is still unclear and currently under debate.

Human brown fat *in vivo* studies have indicated that intracellular triglycerides are depleted during cold stress (Gifford et al., 2016; Lundstrom et al., 2015). However, it is not clear from these studies whether these NEFAs are either directed towards oxidation, released in the blood circulation, or rather re-esterified [triglyceride-fatty acid cycle, (Reshef et al., 2003; Vallerand et al., 1999)]. Other human studies suggest that the lipolysis of intracellular triglycerides is necessary for the activation of BAT thermogenesis during cold stress (Blondin et al., 2017a); nevertheless, the fate of these NEFAs, produced by intracellular lipid breakdown, remains inconclusive. Additionally, the proportional contribution of these NEFAs accounting for BAT oxidative metabolism during cold stress is still speculative and currently there is no available tool to estimate the amount of these consumed lipids.

For BAT metabolism, NEFAs are also extracted into the brown adipocytes from the circulation. These NEFAs are imported into the brown adipocytes with the help of membrane receptor proteins. These receptor proteins include a cluster of differentiation 36 (CD36), FA transport proteins-1 and FA transport proteins-4 (FATP1 & FATP4), (Goldberg et al., 2009; Lobo et al., 2007; Wu et al., 2006). In addition to the free-form NEFA in the blood circulation, the NEFAs are also liberated from the chylomicrons by the activity of LPL. LPL hydrolyses the chylomicrons into NEFA for the brown adipocytes uptake. Once inside the brown adipocytes, these NEFAs can be esterified into triglycerides for storage, or undergo β-oxidation into the mitochondria for cellular respiration. However, these mechanism are not widely explored in humans, and the proportional contribution of circulatory NEFA for BAT thermogenesis remains unclear.

The fate of the glucose after the uptake by the brown adipocyte is also imprecise; the glucose uptake is assumed to represent the thermogenic activity of BAT

during cold stress (Muzik et al., 2013). However, it is unclear whether this glucose is directed towards oxidation, or glycogen formation, or rather directed towards the triglyceride synthesis. The studies in rodents and human adipocytes *in vitro* experiments have indicated that the glucose uptake is predominately directed towards the glycerol-3-phosphate production for triglyceride synthesis (Barquissau et al., 2016; Laplante et al., 2008; Moura et al., 2005).

2.2.4 Circulatory lipid clearance by brown adipose tissue

The rodent studies suggest that brown fat may have the capacity to clear up the excess circulating lipids in the body, and this tissue may act as a protector against hyperlipidaemia (Berbée et al., 2015) and it may also act as a tissue which may protect against the development of atherosclerosis (Hoeke et al., 2016). The cross-sectional human studies show that the presence of BAT in healthy adults is independently linked with low incidence of dyslipidaemia (Shao et al., 2016) and a reduced risk of cardiovascular diseases (Takx et al., 2016). However, in humans no longitudinal studies have been done on the mechanistic role of brown fat for the clearance of excess circulating lipids and glucose. This role of BAT in adult humans is questioned and thus the overall relevance of BAT in the clearance of excess circulatory substrates is not clear. In fact a few studies suggest that the overall consumption of circulatory lipids and glucose by adult human BAT merely represents less than 1% of the systemic turnover of these substrates (Blondin et al., 2015a).

2.2.5 Therapeutic potential of human brown adipose tissue

In addition to the role of brown fat as a protector against hypothermia, BAT has been considered as a potential organ to combat obesity and related metabolic disorders such as type II diabetes mellitus. Scientists have speculated that the activated brown fat can dissipate the excess energy stored in the body as heat, and additionally the conversion of WAT to BAT, a process known as browning of adipose tissue, can be a viable option for the treatment of obesity. Moreover, several researchers are in pursuit of the agents which may selectively activate brown fat since it has been speculated that selective BAT activation is necessary to create a negative energy balance for weight loss without creating any negative

effects on the cardiovascular (Fares, 2013; Florea and Cohn, 2014) and cognitive systems (Moreira and Crippa, 2009).

The data from cross-sectional human studies suggest that the stored lipid content of human BAT is associated with whole-body insulin sensitivity in healthy (Raiko et al., 2015) as well as diabetic and pre-diabetic human subject (Koksharova et al., 2017). Other human studies have suggested that the activation of BAT with cold acclimation reduces the BAT stored lipids, and improves whole-body insulin sensitivity in healthy lean and obese subjects, as well as in patients with type II diabetes mellitus (Blondin et al., 2014; Hanssen et al., 2015b, 2016; Lee et al., 2014). These studies have speculated that BAT may have a role in the regulation of whole-body insulin sensitivity; however, the molecular mechanisms behind this are not known.

Moreover, brown adipose tissue has been speculated to have a contributory role in diet induced thermogenesis (Glick et al., 1981) and further, it is considered as an energy sink in order to maintain the energy balance (Rothwell and Stock, 1979). However, these speculations are based on rodent studies, and the concept of 'diet-induced thermogenesis' as a mechanism for maintaining energy balance in humans is controversial (Kozak, 2010).

2.3 Non-invasive imaging of brown adipose tissue

2.3.1 X-ray computed tomography

X-ray computed tomography (CT) is a widely used medical imaging technique which uses the ionising x-ray radiation to produce cross-sectional images of the body. The image formation in CT is dependent on the x-ray attenuation of the body structures, which is dependent on the underlying density of the scanned tissue (Ciarelli et al., 1991; McBroom et al., 1985). The term used for the CT attenuation of a tissue is radiodensity, and it is quantitatively expressed with CT numbers, called Hounsfield units (HU). The HU of the acquired images are normalised based on the attenuation co-efficient of the water, and HU of water is considered to be zero (0).

Since BAT and WAT have different densities due to the differences in the amount of stored triglycerides, mitochondria, vasculature and water content; therefore, it is reasonable to assume that the differences in tissue densities can be appreciated in the different attenuation values of the CT imaging for BAT and WAT. Since adipose tissue mainly constitutes of the stored lipids, in human studies, the radiodensity of adipose tissue has therefore been speculated to represent the lipid content of the tissue; however, direct evidence is currently missing.

Humans studies utilising CT imaging have found that those adipose tissues which have a higher circulatory glucose uptake also have a higher CT radiodensity (Ahmadi et al., 2013; Baba et al., 2010; Hu et al., 2010). Additionally, it was also noticed that the CT radiodensity of BAT increases under cold stress, suggesting consumption of the stored triglycerides (Ouellet et al., 2012). Furthermore, pharmacologically blocking the lipolysis in human adipose tissues abolishes the cold-induce change in BAT radiodensity, also suggesting that BAT radiodensity represent stored triglycerides (Blondin et al., 2017a). Additionally, several other studies have assumed that the radiodensity of BAT represent the amount of stored triglycerides (Hanssen et al., 2015b, 2016; Lee et al., 2014).

2.3.2 Magnetic resonance imaging and magnetic resonance spectroscopy

Magnetic resonance imaging (MRI) has provided an approach to the imaging of BAT without ionising radiation and with a superior imaging resolution compared to PET. The MRI, with the aid of different imaging protocols can assist in differentiating WAT from BAT (Holstila et al., 2013, 2017), and additionally, it also has the possibility to provide an insight into the blood flow of the tissue (Chen et al., 2013). Additionally, magnetic resonance spectroscopy (MRS) can aid in determining the composition of BAT, in terms of amount of triglyceride content; and in addition, it has been shown that MRS can also provide an insight into the temperature of the tissue (Koskensalo et al., 2017).

The studies in adult humans using MRI and MRS imaging methods show that the glucose consumption by BAT is linked with the fat fraction of the tissue (Holstila et al., 2017; McCallister et al., 2017).

2.3.3 Positron emission tomography

Positron emission tomography (PET) is a non-invasive medical imaging technique which utilises the short-half life positron emitting radionuclide, incorporated into the biological molecules, to image the molecular functions in the human body. The positron emitting radionuclides (^{18}F, ^{11}C, ^{15}O) are produced with a cyclotron and these radionuclide are combined with the other molecules using various labelling methods. The nature of the molecular mechanisms that can be studied with PET depend upon the radiotracer used in the PET imaging. The most common method of incorporating a radiotracer into the human body is via direct administration into the blood (intravenously). However, other methods can also be employed, for example, many radiotracers can be given orally, and additionally, the administration of gaseous form radiotracers into the body is also possible via inhalation. The route of the administration of radiotracers into the body also depends upon the intended molecular mechanism to be studied. Subsequent to administration, the radiotracer circulates (via the blood circulation) and is distributed to the organs and tissues. The rate of accumulation and turnover of the radiotracer in a certain organ or tissue depends on the specific nature of the radiotracer as well as the underlying specific molecular mechanism occurring in the respective area of the body.

Once a radiotracer is administered, the radionuclide continues to undergo a nuclear decay, and thus it continuously emits positrons. The emitted positrons, possessing a positive charge, collide with the electrons and as a result, both annihilate. The process of annihilation converts the mass of these colliding particles into energy ($e = mc^2$) and consequently two gamma photons are emitted travelling in opposite direction to each other, from the point of annihilation. These gamma photons are detected by the PET detectors which are designed in a way that they surround the supine body of the patient/subject inside the PET scanner (Figure 5). The scanner estimates the 'line of response' between the two opposite simultaneous detections and thus the accumulation or high turn-over of a radiotracer in a part of the body is detected as a numerous annihilations. The obtained raw data by the detectors is processed by the computers to form a reconstructed tomographic image (Cherry and Dahlbom, 2006; Saha, 2010).

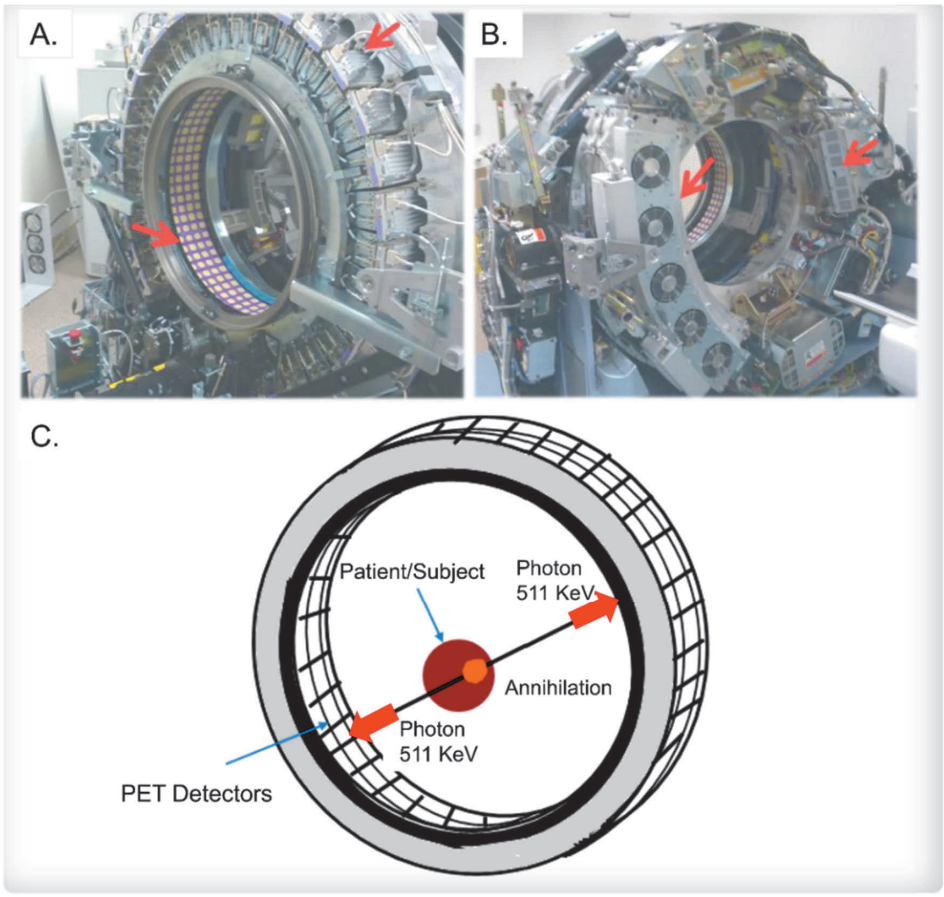

Figure 5. A PET-CT scanner and the principle of PET imaging
A & **B**: Photographs of the exposed gantry of PET-CT scanner (General Electric, Discovery 690 PET-CT Scanner). **A.** PET assembly of the scanner; the red arrows point to PET detectors (bottom left) and photo multiplier tubes (top right). **B.** CT assembly of the scanner; red arrows point to x-ray tube (right) and x-ray detectors (left). Image courtesy: Tony Shepherd, Turku PET Centre, Turku University Hospital (TYKS), Turku, Finland. **C.** A diagrammatic illustration of the PET scanner. The gamma photons are produced as a result of annihilation, and they are detected in coincidence by the PET detectors surrounding the patient/subject, and the simultaneously annihilating photons detected by PET detectors in an opposite direction are recorded as one single event.
Figure modified from U Din (2013)

PET imaging has gained popularity due to the unique utility in the field of oncology where PET images provide a spatial map of the body highlighting the

areas with greater glucose metabolism (static PET imaging). In addition to provide a spatial map, PET has the added ability to reveal the metabolism of the tissues in temporal dimension as well (Muzi et al., 2012). This PET image acquisition protocol is termed as dynamic imaging/scanning, and it has the added ability to quantify the metabolic rates of the tissues (Mazoyer et al., 1986). For example, with the [^{18}F]2-fluoro-2-deoxy-D-glucose radiotracer ([^{18}F]FDG) the tissue-specific metabolic rate of glucose consumption can be determined (Wienhard et al., 1985). In the studies examining BAT with PET imaging, researchers widely report the static accumulation of radiotracer in terms of the standardised uptake value (SUV); though this method has some inherent limitations (Keyes, 1995). Only a few research groups have examined the rate of BAT metabolism which widens the overall interpretation of the results (Ouellet et al., 2012; Virtanen et al., 2009).

2.4.3.1 PET imaging of BAT to investigate glucose metabolism

PET imaging, using the glucose analogue radiotracer, is employed to study the glucose metabolism of the tissue. The *in vivo* detection of BAT in adult humans has only been possible with the PET imaging using the most commonly clinically utilised radiotracer, [^{18}F]FDG (Cypess et al., 2009; van Marken Lichtenbelt et al., 2009; Virtanen et al., 2009). Several studies have utilised this PET tracer to detect BAT (Cohade et al., 2003), compare BAT and WAT glucose activity (Ahmadi et al., 2013) and as well to estimate the rate of the glucose uptake by BAT in different metabolic states (Blondin et al., 2015; Orava et al., 2013, 2011).

Since the FDG molecule is the analogue for the glucose molecule, it accumulates in the area of the body with higher glucose metabolism. The FDG molecule follows the same transportation mechanism into the brown adipocyte as a glucose molecule (section 2.2.2 & 2.2.3). Once inside the adipocytes, the FDG is phosphorylated to FDG-6-phosphate by hexokinase. Contrary to the glucose-6-phosphate, the FDG-6-phosphate cannot further undergo glycolytic pathway and thus it becomes irreversibly trapped in the tissue. The accumulated FDG represent the extent of the glucose uptake into the tissue (Phelps, 2000). Due to the wide availability of [^{18}F]FDG for clinical imaging, the [^{18}F]FDG has been the most commonly used radiotracer in the field of BAT research; therefore, it has become a standard in human BAT imaging with PET-CT. However, the practise to adopt this as a standard for the localisation of BAT is questionable.

2.4.3.2 PET imaging of BAT to investigate fatty acids metabolism

A few studies have also used the fatty acid based tracer, 14(R,S)-[^{18}F]fluoro-6-thia-heptadecanoic acid, commonly termed [^{18}F]FTHA, to study the metabolism of the circulatory (Ouellet et al., 2012) and dietary (Blondin et al., 2017a) fatty acids in brown fat thermogenesis. The accumulation of this tracer, subsequent to administration directly into the blood, represents the uptake of the circulatory NEFA into the tissue. Once administered orally, it may represent uptake of all dietary fatty acids into the tissue (Blondin et al., 2017b).

2.4.3.3 PET imaging of BAT to investigate blood perfusion

The blood perfusion into BAT has been studied with the administration of the [^{15}O]H_2O radiotracer. It has been shown that cold stress increases the blood perfusion of BAT in humans (Muzik et al., 2013; Orava et al., 2011). Additionally, the effect of insulin stimulation on BAT blood perfusion has also been studied, and it has been found that the blood perfusion is not influenced by the insulin stimulation (Orava et al., 2011). The increased perfusion in the brown fat, during the cold stress, is assumed to be due to the increased demand of the substrates and oxygen required by the BAT for thermogenesis. Additionally, the increased BAT perfusion can also likely be caused by need to distribute the produced heat by the BAT to the rest of the body.

2.4.3.4 PET imaging of BAT to investigate oxidative metabolism and oxygen consumption

PET imaging with [^{11}C]acetate and [^{15}O]O_2 has the potential to provide insight into the mitochondrial respiration activity of the tissue.

The [^{11}C]acetate provides the evidence of the CAC in the mitochondrial respiratory reaction and thus it acts indirectly as a marker for the oxidative metabolism of the tissue. The acetate molecule once converted to acetyl-CoA enters the CAC where it is oxidised to CO_2 (Buxton et al., 1988). However, it has been suggested that the metabolic fate of [^{11}C]acetate in adipose tissue may not always be entering the CAC. The [^{11}C]acetate may also becomes incorporated into lipids (Klein et al., 2001). BAT studies in adult humans using [^{11}C]acetate

have suggested that the oxidative metabolism of BAT increases during mild cold stress (Ouellet et al., 2012), the cold acclimation further increases the oxidative metabolism of BAT (Blondin et al., 2014), the patients with type II diabetes do not have a defect in the oxidative metabolism of BAT (Blondin et al., 2015b), and the inhibition of lipolysis in BAT also supresses the oxidative metabolism (Blondin et al., 2017a).

The $[^{15}O]O_2$ radiotracer is administered in the body via inhalation and it provides a direct measurement of the oxygen consumption by the tissue. Since the half-life of the oxygen-15 is very short (122.2 sec), the studies with $[^{15}O]O_2$ therefore require an on-site cyclotron closer to the PET scanner, and a very delicate setup for the inhalation of this radiotracer. Additionally, since the gases diffuse quicker than the liquids the detection of this radiotracer over the temporal dimension is therefore also challenging. Nevertheless, the use of $[^{15}O]O_2$ radiotracer for the measurement of the metabolic rate of oxygen consumption of brain has been validated (Kudomi et al., 2013; Mintun et al., 1984; Ohta et al., 1992).

In the context of human BAT, the metabolic rate of BAT measured by oxygen consumption can reveal the overall energy expending potential of this tissue. Hence, the utility of $[^{15}O]O_2$ radiotracer for human BAT research is immense. However, due to the complexity of the $[^{15}O]O_2$ PET imaging, it has not been widely used. Thus, this thesis work focused on imaging human BAT with $[^{15}O]O_2$ radiotracer to examine the oxidative metabolism. Over the course of this thesis work only one study by Muzik et al. (2013) appeared on this topic on the scientific front. The study has shown that the oxygen consumption of adult human BAT increases after the 20 minutes of cold stress, and BAT has limited energy expending potential during cold stress.

2.4.3.5 Estimate of BAT mass with PET imaging

In addition, to understand the substrate metabolism of BAT in humans, scientists have also been intrigued to know the approximate mass of BAT in an adult human body. Various studies have been carried out with the idea that BAT displays an increased substrate (mainly glucose) metabolism when stimulated, and CT/MRI can confirm that the suspected tissue is likely an adipose tissue. However, the limitation of estimating brown fat mass in adult humans with PET-CT is the low PET sensitivity and spatial resolution, and additionally, non-

availability of brown fat specific PET radiotracers. The traditionally used [^{18}F]FDG radiotracer merely highlight the adipose tissue areas with comparative higher glucose metabolism; therefore utilisation of [^{18}F]FDG radiotracer for the estimation of the amount and prevalence of BAT is likely to lead to a gross underestimate. Nevertheless, the total estimated BAT mass from these approaches appears to be less than 300 grams.

The brown fat mass/volume determined by these technique have been shown to be linked with the peptides secreted by the gastrointestinal system (Chondronikola et al., 2017) and thus speculated to have a role in appetite regulation. Additionally, BAT mass has been shown to be linked inversely with lean mass, and positively with irisin and thyroid hormones (Singhal et al., 2016).

3 AIMS OF THE STUDY

1. To evaluate the feasibility of the measurement of oxygen consumption of human brown fat with [^{15}O]O_2 PET imaging (I)

2. To investigate the effect of cold stimulus and meal ingestion on the oxidative metabolism of brown fat in adult humans (I – II).

3. To determine whether brown fat has a significant contribution towards whole-body energy metabolism, particularly in cold-induced (CIT) and meal-induced thermogenesis (MIT) (I – II).

4. To investigate the utility of x-ray computed tomography (CT) imaging in characterising human brown fat (III).

5. To examine the capacity of x-ray computed tomography (CT) imaging for studying the metabolism of human brown fat (III).

4 MATERIALS AND METHODS

4.1 Study subjects

The recruitment of study subjects was arranged by the investigators at Turku PET centre and thus healthy adult humans of both genders were enrolled by means of newspaper and electronic advertisements. The study subjects were screened based on the following exclusion criteria,

- Previous participation in clinical trials requiring ionising radiation scans
- Pregnancy or lactation
- Regular smoking
- Hypertension (blood pressure > 160/100 mmHg)
- Hypo- or hyper- thyroidism
- Diabetes mellitus
- Abnormal oral glucose tolerance test (2h OGTT > 7.8 mmol/L)
- Abnormal cardiovascular status (arrhythmia and/or long QTc in ECG, abnormal cardiac murmur, previous history of cardiovascular disease)
- Malignancies

In addition to these screenings, the metabolic health of the all the study subjects was further assessed by performing a physical examination in a fasting state to measure weight, waist circumference, hip circumference, height, and body fat percentage (Omron BF400, Omron Healthcare). Whole-body insulin sensitivity (M-value) was measured using a hyperinsulinemic euglycemic clamp technique (DeFronzo et al., 1979). Additionally, a routine blood test (i.e., complete blood count, liver and thyroid function tests, creatinine, K, Na, and lipids) was also conducted. All study subjects included in the studies were metabolically healthy and did not have any significant medical condition. The anthropometric parameters of the study subjects have been provided in Table 1.

Table 1. Anthropometric details of the human study subjects in study I - III

Studies		n	Gender	Age (years)	BMI (kg/m^2)	Waist (cm)
Study I		7	2 F / 5 M	36 ± 11	25.5 ± 3.3	90.4 ± 10.4
Study II	Control group	9	4 F / 5 M	36 ± 9	26.1 ± 3.1	89.9 ± 9.2
	Experimental group	16	12 F / 4 M	35 ± 11	27.3 ± 3.9	92.9 ± 16.0
Study III		66	45 F / 21 M	39 ± 10	25.4 ± 4.4	86.3 ± 15.8

The study participants in Study I also acted as part of the controls in Study II, while Study III also included the participants of both Study I and II.

4.2 Study designs

4.2.1 CIT and oxidative metabolism of BAT at RT and mild cold (I)

Subjects underwent two scanning sessions; one of the scanning sessions was performed at room temperature and the other during acute cold exposure. Scanning sessions were organised on separate days, in a random order, with the minimum interval between the sessions being one week. Studies were performed after overnight fasting. All scans were performed at the same time of day in order to minimise any possible effect caused by individual circadian rhythm. Cold exposure was started 2 hours prior to the scan using cooling blankets and cooling was continued during the PET scanning. Room temperature (RT) was maintained at approximately 22 °C. The study design has been diagrammatically shown in Figure 6.

4.2.2 MIT and oxidative metabolism of BAT in postprandial state (II)

Participants underwent scanning sessions which only differed by the external stimuli; the experimental group was scanned at two different known thermogenic physiological conditions, cold and after taking a meal (Figure 6), while the control group underwent scanning with cold stimulus (positive control) and without cold stimulus at room temperature of ~ 22°C (negative control). Each subject participated in two scanning sessions which were organised on two

different days, while the minimum duration between the two sessions was one week. In all the scanning sessions, the subjects fasted overnight and the scans were performed at the same time of day in order to minimise any possible effects of individual circadian rhythms on body metabolism. In the cold stimulus experiments, the subjects were given cold stimulus using cooling blankets for two hours prior to the start of the scan and the cold stimulus continued during the scans as well. In the standardised-meal experiments, the subjects ingested a meal of approximately 542 kcal, of which 58 % were carbohydrates, while 25% and 17% belonged to fats and proteins, respectively. The study design has been diagrammatically shown in Figure 6.

4.2.3 Non-invasive characterisation of BAT using CT radiodensity (III)

The subjects were scanned with PET-CT, in an individualised cold stimulus setting, where part of the study subjects were scanned with a glucose analogue [^{18}F]FDG radiotracer (n = 26) and part of the study subjects were imaged using a fatty acid analogue [^{18}F]FTHA radiotracer (n = 40). At the same scanning setting [^{15}O]H_2O PET scans were also performed for the measurement of tissue retained arterial blood volume (V_A). The CT and [^{15}O]H_2O PET scanning was repeated, on a separate day, at RT (22 ºC) with half of the study subjects (n = 33) as a comparative secondary parameter; while cold stimulated BAT CT radiodensity being a primary evaluated parameter of the current study. Blood samples were drawn during the PET-CT scans to measure plasma concentration of glucose, non-esterified fatty acids (NEFA), triglycerides and thyroid hormones. Indirect calorimetry, using Deltatrac II Datex-Ohmeda, was performed during the PET-CT sessions to measure whole-body energy expenditure (EE) according to the Weir equation (Weir, 1949). During the cold stimulus PET-CT scanning sessions, the skin temperature of the subjects was monitored using a digital thermometer (Art.183, Termometerfabriken Viking AB, Eskilstuna, Sweden) where the temperature sensing probe was attached to the lateral abdominal skin surface. Additionally, in a separate scanning session, magnetic resonance proton spectroscopy (^{1}H-MRS) in the supraclavicular fat depot was performed at ambient RT for the determination of stored triglyceride. All the scanning sessions were performed after overnight fasting. The scanning sessions were organised on separate days, in a random order, with the minimum interval between the

sessions being one week. The study design has been diagrammatically shown in Figure 6.

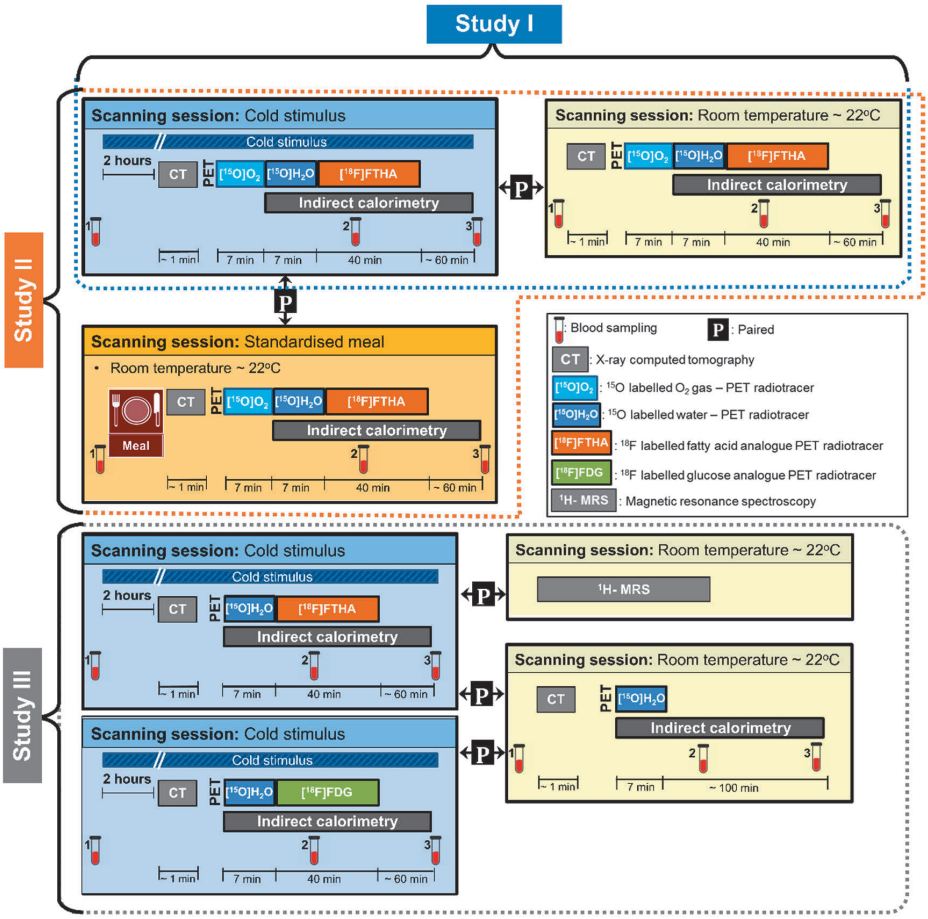

Figure 6. Diagrammatic representation of study designs I - III

The scanning protocol utilised to measure whole-body energy expenditure, BAT oxidative metabolism, blood flow, NEFA uptake, glucose uptake, tissue retained blood volume, radiodensity, and triglyceride content at room temperature (I), during cold stimulus (I-III) and/or after the meal ingestion (II).

4.3 Cold exposure (I – III)

In the studies involving cold exposure, the cooling of the subjects was started 2 hours prior to the scan using cooling blankets (Blanketrol III, Cincinnati Sub-Zero, Cincinnati, USA, Figure 7A) and cooling was continued during the PET scanning. The cooling was started with the temperature of the water circulating the cooling blanket set to 4 - 6 ºC; this temperature was gradually raised once overt shivering was perceived by the subjects, either reported by the subject themselves or visually observed by the investigator. Figure 7B shows the temperature of the cooling blankets, the data set has been divided to show the differences between the lean and overweight-obese subjects.

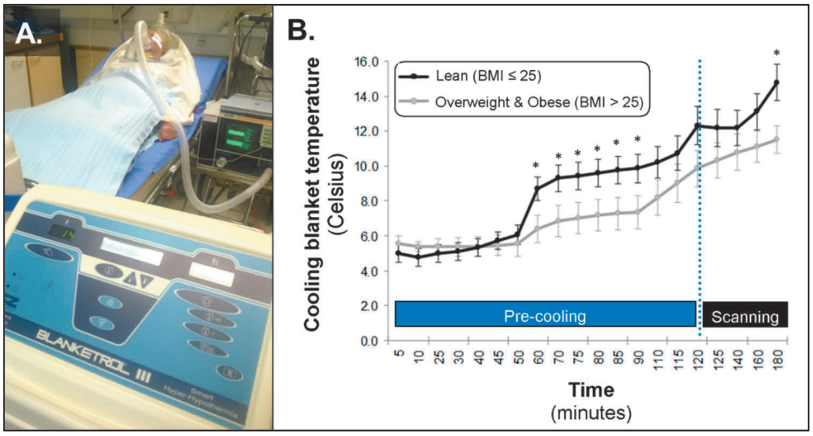

Figure 7. Cold exposure induced in the study subjects

A. The cooling blankets used for the giving the cold stimulus to the study subjects. **B**. The temperature of the cooling blankets for delivering non-shivering cold stress to the subjects. The temperature of the cooling blanket was raised once overt shivering was observed. Significant differences in the cooling blanket temperatures, after 1 hour of cooling, were observed when the subjects were divided into groups based on BMI (lean: BMI ≤ 25; overweight-obese: BMI > 25). Lean individuals reported shivering earlier than overweight-obese participants; therefore, the overall temperature of the cooling blanket was lower (colder) for overweight-obese participants. * $p <$ 0.05, independent sample Student t-test.

4.4 Skin temperature measurements (I – III)

The skin temperature of the subjects was also monitored during scanning, using a digital thermometer (Art.183, Termometerfabriken Viking AB, Eskilstuna, Sweden); the temperature sensing probe was attached to the lateral abdominal skin surface.

4.5 Standardised meals (II)

The standardised meals ingested by the study subjects prior to the scanning in the Study III consisted of approximately 542 kcal, of which 58 % were carbohydrates, while 25% and 17% belonged to fats and proteins, respectively. Table 2 shows the contents of the meal and nutritional values.

Table 2. Description of ingested food

Food	Quantity	Energy (kcal)			
		Total	Carbohydrate	Fat	Protein
Vegetable lasagne	200 g	226	106.2	85.9	33.9
Milk	2 dl	84	41.2	1.7	41.2
Salad	50 g	8	5.5	0.9	1.6
Salad dressing	10 g	27.4	6.6	20.3	0.5
Rye bread	1 piece	99.2	80.4	6.0	12.9
Margarine	5 g	17.8	0.0	17.8	0.0
Blueberry soup	1 dl	79.5	75.5	3.2	0.8
Total (kcal)		542	293	134	91
Percentage (%)			58	25	17

4.6 PET-CT Imaging

4.6.1 Production of PET tracers

Low-energy deuteron accelerator Cyclone 3 (Ion Beam Application Inc., Louvain-la-Neuve, Belgium) was used for the production of $[^{15}O]O_2$. $[^{15}O]$ isotope (physical $t_{1/2}$ 123 s) was produced by the $[^{14}N]$ (d,n) $[^{15}O]$ nuclear

reaction on natural nitrogen gas (Strijckmans et al., 1985). Radiowater [^{15}O]H_2O was produced using Hidex Radiowater Generator (Hidex Oy, Turku, Finland). [^{18}F]FDG and [^{18}F]FTHA (physical $t_{1/2}$ 110 mins) were synthesised in accordance with standard operating procedure of Turku PET centre (Hamacher et al., 1986).

4.6.2 PET-CT image acquisition

Subjects were placed supine in a head-first position inside the PET-CT scanner (Discovery 690 PET-CT scanner; General Electric Medical Systems, Milwaukee, WI, USA, PET voxel size = 3.64 x 3.64 x 3.27 mm) while the level of the clavicles was set as the centre of the axial field of view (AFOV). A comfortable, relaxed position for the subjects was ensured in order to avoid any tension in the neck muscles, and the arms were placed next to the body. The positioning of the subjects within the scanner was kept identical irrespective of the cooling protocol utilised. Scanning started with an attenuation correction transmission CT scan. The CT scans were performed using low-dose scanner settings where the x-ray tube current was approximately 50 mA and the tube voltage was 120 kVp. The CT scan was followed by dynamic emission PET scans using different radiotracers i.e. [^{15}O]O_2, [^{15}O]H_2O, [^{18}F]FTHA and [^{18}F]FDG.

In the [^{15}O]O_2 scans, the subjects were given radioactive oxygen gas (509 ± 37 MBq) using a plastic mask with a single deep inhalation and scanning was started simultaneously; 20 frames of variable lengths were acquired over a period of 7 minutes (6 × 5sec, 6 × 15sec, 6 × 30sec, 2 × 60sec).

The radiowater scans were conducted by intravenous injection of [^{15}O]H_2O (493 ± 35 Mbq) into the left antecubital vein and immediately starting the scanning, following to the injection, using 20 frames with a dynamic acquisition protocol (6 × 5sec, 6 × 15sec, 6 × 30sec, 2 × 60sec).

The [^{18}F]FDG and [^{18}F]FTHA PET scans were performed using a dynamic acquisition protocol (40 min; 4 x 30 s, 1 x 60 s, 1 x 120 s, 3 x 300 s, 2 x 600 s) following the administration of approximately 185 MBq of radiotracer into the left antecubital vein.

4.6.3 PET image reconstruction

All quantitative corrections were applied to the PET image data, including detector normalisation, dead-time, radioactive decay, randoms, attenuation and scatter. Images were reconstructed using iterative 3D-OSEM (GE Vue Point HD-S) reconstruction using 24 subsets and 2 iterations. All images were filtered using 6.4 mm Gaussian post-filter. Due to the presence of large in-FOV and out-FOV activity in the first frames in the [^{15}O]O_2 inhalation study, a clinically implemented scatter limit was applied (GE Quantitative Scatter Limit). The procedure is necessary to prevent scatter overestimation due to large in-FOV and out-FOV activity (Hori et al., 2014).

4.7 PET-CT image analysis

4.7.1 Volume of interest (I – III)

The volume of interests (VOIs) in BAT were drawn manually on the supra-clavicular fat depots on the fused PET-CT images by taking into account the CT Hounsfield unit (HU) value of the voxels within -50 to -250 HU range. White adipose tissue VOIs were drawn on the posterior subcutaneous neck area. For skeletal muscle, VOIs were drawn on deltoid, trapezius, levator scapulae, splenius cervicis and pectoralis major muscles. For all the radiotracers used, arterial input function was determined by drawing a VOI comprising of 70 – 100 voxels on the arch of the aorta on the fused PET-CT images.

4.7.2 Measurement of blood perfusion (I- III) and tissue retained blood volume (III)

Blood perfusion and tissue retained blood volume (V_A) was calculated from [^{15}O]H_2O PET scans by assuming a one-tissue compartmental model as follow,

$$C_T(t) = K_1^W \cdot C_A(t) \otimes e^{-K2 \cdot t} + V_A \cdot C_A(t)$$

Where C_T is the tissue time activity curve, C_A is the input function and V_A is the arterial blood volume. The K_1^w, k_2, and V_A, values were estimated by an optimisation procedure (Gauss-Newton method).

4.7.3 Measurement of tissue oxygen consumption

The tissue oxygen consumption was calculated by incorporating the time activity curves (TACs) of $[^{15}O]O_2$ and $[^{15}O]H_2O$ PET scans by assuming a one-tissue compartmental model as follow,

$$C_T(t) = K_1^O \cdot C_A^O(t) \otimes e^{-K2 \cdot t} + K_1^W \cdot C_A^W(t) \otimes e^{-K2 \cdot t} + V_0 \cdot C_A^0(t)$$

where C_T is the tissue TAC, C_A^O and C_A^w are the input functions for oxygen and water, respectively. For the estimation of oxygen and water content, the aorta TAC was separated for each component according to the mathematical model described by Iida et al. (1993). V_0 is the arterial blood volume. The first term in the equation expresses the kinetics of oxygen and the second that of water, namely recirculation water. The K_1^o, and V_0, values were estimated by an optimization procedure (Gauss-Newton method), by inputting the obtained K_1^w and k_2 from the water data (Kudomi et al., 2013). Subsequently, the oxygen consumption in the specific tissue was calculated as a product of K_1^o and the arterial oxygen concentration $^aO_2$ (mlO_2/100ml). The arterial concentration of oxygen was considered to be 19.8 mL per 100 mL of blood volume. Oxygen consumption for muscles was calculated by taking into account the oxygen binding in myoglobin (Nuutila et al., 2000; Oikonen et al., 1998).

4.7.4 Measurement of tissue non-esterified fatty acids uptake (I – III)

The net influx rate (K_i) of $[^{18}F]$FTHA was calculated from tissue specific TACs obtained from $[^{18}F]$FTHA PET scans using the Patlak model (Patlak and Blasberg, 1985). The image derived plasma input function was corrected for metabolites which were measured from samples acquired during the scanning. Net NEFA uptake was subsequently calculated by multiplying K_i with plasma NEFA concentration measured during the $[^{18}F]$FTHA PET scanning and divided by lumped constant.

4.7.5 Measurement of tissue glucose uptake and [^{18}F]FDG SUV (III)

The net influx rate (K_i) of [^{18}F]FDG was calculated from tissue specific TACs obtained from [^{18}F]FDG PET scans using the Patlak model (Patlak and Blasberg, 1985). Image derived whole-blood TAC was converted to plasma input TAC by taking into account the haematocrit and continuing accumulation of [^{18}F]FDG in red blood cells. The net glucose uptake was subsequently calculated by multiplying K_i with plasma glucose concentration measured during the [^{18}F]FDG PET scanning and diving by the lumped constant. A lumped constant of 1.14 was used for adipose tissue (Virtanen et al., 2001) and 1.20 for skeletal muscles (Peltoniemi et al., 2000). For the purpose of comparison with tissue glucose uptake, we calculated the tissue standardised uptake values (SUVs). The SUVs were calculated by taking into account tissue radioactivity at the 30-40 mins PET frame, injected radioactivity dose, and body mass.

4.7.6 Tissues mass calculation (I - II)

BAT mass, in the cervico-upper thoracic region, was estimated on fused PET-CT images by first thresholding all CT voxels between a range of -50 to -250 HU at all potential cervico-upper thoracic BAT sites (cervical, supraclavicular, and axillary adipose depots). The acquired voxels underwent further thresholding and all voxels with less than 0.7 µmol/100g/min NEFA uptake on parametric cold-exposure [^{18}F]FTHA PET images were excluded. Finally, the volume of all these voxels (cm^3) was converted into mass by assuming the density of BAT to be 0.92 g/cm^3.

Muscle mass in the cervico-upper thoracic region was calculated from the CT images by thresholding all CT voxels at all muscle sites between 0 to +250 HU. Afterwards, the volume of all these voxels (cm^3) was converted into mass by assuming the density of the muscle to be 1.06 g/cm^3.

4.7.7 Hounsfield unit measurements (I - III)

Carimas 2.8 software (Turku PET Centre, Turku, Finland) was used to analyse all the acquired CT images. On the CT images all potential BAT locations within the cervico-upper thoracic region were marked and all voxels between -250 HU

to -50 HU were thresholded (Figure 8). We also examined a somewhat wider range for the HU threshold (-250 to 0 HU); however, the visual inspection of those voxels revealed inclusion of non-adipose tissue structures, hence a threshold upper-bound value of -50 HU was found to be reasonable. Muscles volumes of interests (VOIs) were drawn at the deltoid and pectoralis major region; and anterior subcutaneous fat in abdominal region was considered as WAT. Afterwards, mean Hounsfield units (HU) of all the regions of interest were calculated and compared.

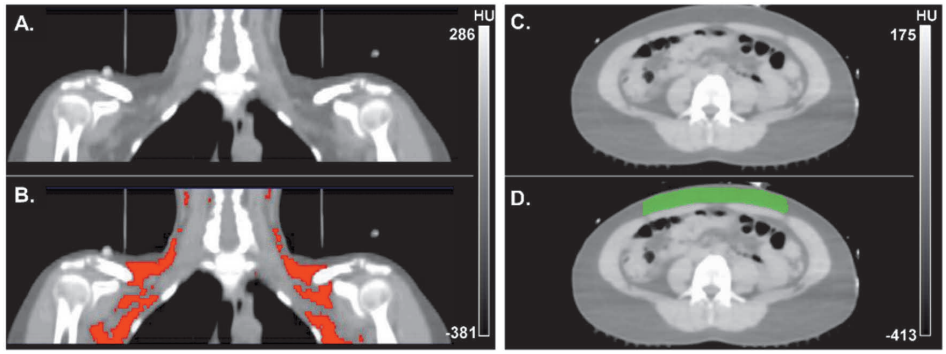

Figure 8. CT image analysis for the calculation of adipose tissue HU
A: Representative single coronal CT image of the cervical upper thoracic region. **B**: Red areas show segmented BAT areas obtained after thresholding voxels between -250 HU to -50 HU. **C**: Representative single axial image of the abdominal region. **D**: Green areas show segmented anterior subcutaneous WAT in abdominal region for the calculation of mean HU. Modified from U Din et al. (2017).

4.7.8 Tissue specific DEE measurements (I - II)

Tissue specific daily energy expenditure (DEE) was calculated from oxygen consumption (MRO_2) according to the formula below,

$$DEE\ tissue\ (kcal/day) = MRO_2\ (mL/100g/min) \times tissue\ mass\ (100g) \times\ 0.0048\ (kcal/mL) \times\ 1440\ (min/day)$$

The energy (kcal) produced per millilitre of oxygen consumption was assumed to be for a respiratory quotient (RQ) of 0.80 (4.801 kcal/ litre O_2 consumed) (Leonard, 2010).

4.8 ^{1}H- MRS

^{1}H-MRS was performed using a pointed- resolved spectroscopy (PRESS) sequence with a repetition time (TR) of 3000 ms, an echo time (TE) of 25 ms and a number of signal averages (NSA) of 4. A sample frequency 1000 was used with 2048 samples. T2 correction was not applied. The size of the voxel was optimized and adjusted for each subject in order to avoid surrounding muscles, and 4 saturation bands were used. Typical voxel size was 10 mm x 10 mm x 12 mm. Scout images with good resolution were acquired for the placement of the spectroscopy voxel. An expert physician specialised in BAT imaging (KAV) located the BAT, based on previous PET studies and general knowledge of BAT anatomy. Great care was taken to place the voxel inside the fat deposit and to avoid all contamination by muscle tissue or vessels. The obtained ^{1}H-MRS data were analysed using the LCModel.

4.9 Indirect respiratory calorimetry (I – III)

Whole body resting energy expenditure (EE) and whole body substrate utilisation rates were measured using an indirect respiratory calorimetry technique (Deltatrac II, Datex-Ohmeda) performed during the scanning sessions for approximately 100 - 120 minutes. Measurements were excluded from the analyses if they deviated more than 1.5 SD from the mean rate of oxygen consumption (vO_2), rate of carbon dioxide production (vCO_2), EE or respiratory quotient values, caused by irregular breathing. The first 30 minutes of the calorimetry data was also excluded. Whole body resting energy expenditure, respiratory quotient and substrate utilisation rates were calculated using vO_2 and vCO_2 according to the Weir equation (Weir, 1949) and manufacturer's equations (Meriläinen, 1987) using Matlab (Version: R2011a). Protein oxidation was accounted for in the equations by considering urinary nitrogen to be 13 g/24 h. Whole body resting energy expenditure and substrate oxidation rates were divided by fat-free mass in order to compare different subjects; the percentage fat

(%) was measured with a bioimpedance based method (Omron BF400, Omron Healthcare).

4.10 RNA isolation and next generation sequencing (II)

Next generation sequencing was performed on the paired biopsy samples of BAT and WAT obtained from the supraclavicular region. Deep-frozen adipose tissues (approx. 30-120 mg) were homogenised in 1 ml TRIsure (Bioline, London/UK) using a dispersing instrument (Ultra-Turrax D-1, Miccra GmbH, Mühlheim/Germany). RNA was prepared, further purified by spin columns (SV Total RNA Isolation System, Promega, Fitchburg WI/USA) and finally eluted in 50 µl water. The RNA concentration was determined photometrically (Nanodrop ND-1000, Peqlab, Erlangen/Germany). Samples were diluted to a concentration of 25-500 ng/µl, denatured for 2 min at 70°C and RNA integrity determined (Bioanalyzer 2100, Agilent Technologies, Santa Clara CA/USA). The RNA integrity number was not determinable in 1 out of 30 samples and ranged from 3.1 to 8.7 in all other samples. The percentage of fragments with >200 nucleotides (DV200) ranged from 60% to 96%. Accordingly, sequencing libraries were prepared by enriching coding RNA to efficiently compensate for degradation (TruSeq RNA Access Coding Transcriptome, RS-301-2001, Illumina San Diego CA/USA). Libraries were sequenced (HiSeq 2500, Illumina) employing appropriate consumables (HiSeq SBS Kit v4, HiSeq SR Cluster Kit v4, Illumina) to a very high depth of 30.2-160.2 million reads per sample. Reads were mapped by a dedicated software platform (Genome Mining Station, Genomatix München/Germany) resulting in 21.2-111.7 uniquely mapped, coding reads and further analysed (Genome Analyzer, Genomatix). Data is presented as 'reads per 1kb transcript length per million mapped reads' (RPKM) and refers to NCBI Reference Sequence Database (RefSeq) transcripts of a given gene.

4.11 Blood measurements

Plasma insulin, TSH, free plasma T4 and free plasma T3 concentrations were measured using the electrochemiluminescence immunoassay technique (Modular E180 automatic analyser, Roche Diagnostics GmbH). The plasma concentrations of total cholesterol, high density lipoprotein (HDL) cholesterol, and triglycerides

were measured photometrically (Modular P800, Roche Diagnostics GmbH). The plasma concentration of low-density lipoprotein (LDL) was calculated using the Friedewald equation (Friedewald et al., 1972). The concentration of NEFA in the serum was determined photometrically (NEFA C, ACS-COD, Wako Chemicals GmbH; Modular P800, Roche Diagnostics GmbH). The plasma glucose concentration was determined by a glucose oxidase method (Analox GM9 Analyzer, Analox Instruments)

4.12 Statistical analysis (I – III)

Statistical analyses were performed using IBM SPSS Statistics (version 22). In case of normally distributed data, the paired sampled Student's t-test was used to compare paired values, whereas an independent sample t-test was used to compare unrelated values. In cases where the data set(s) were not normally distributed, a Wilcoxon signed-rank test and Mann–Whitney *U* test were used for paired and unpaired values, respectively. Pearson's correlation was used for normally distributed data sets, and a Spearman's correlation test was used where the data failed the normality test. Multivariate linear regression analysis was conducted to check whether the relationships between BAT radiodensity and whole-body insulin sensitivity, biochemical markers and anthropometric measurements were independent of any covariates (III). Receiver operating characteristic (ROC) plots were used to find an optimal cut-off limit on the HU scale for the differentiation of BAT from WAT (Zweig and Campbell, 1993) (III). A two tailed *p*-value of less than 0.05 was considered as statistically significant (I – III). Effect sizes (Cohen's *d*) were calculated using an online statistical calculator (Ellis, 2009) (III).

4.13 Ethics

A written informed consent was obtained from all study subjects prior to inclusion in the studies. All studies were approved by the ethical review committee of the Hospital District of Southwest Finland and carried out according to the principles of the Declaration of Helsinki, GMP and GCP guidelines.

5 RESULTS

5.1 Oxidative metabolism of BAT at RT, cold and after a meal (I – II)

The mild cold stress and the ingestion of a carbohydrate dominant mixed meal increased the oxygen consumption and blood flow of human supraclavicular BAT. BAT had higher oxygen consumption than WAT during the cold stress and after the ingestion of a meal. There was no significant difference between either oxygen consumption or blood flow of BAT between cold stimulus and meal ingestion.

In mild cold stress in addition to BAT, several muscles of the cervico-thoracic region showed an increase in oxygen consumption and blood flow compared to room temperature conditions. Figure 9 shows the results of BAT oxygen consumption and blood flow at room temperature, during cold stress and after meal ingestion.

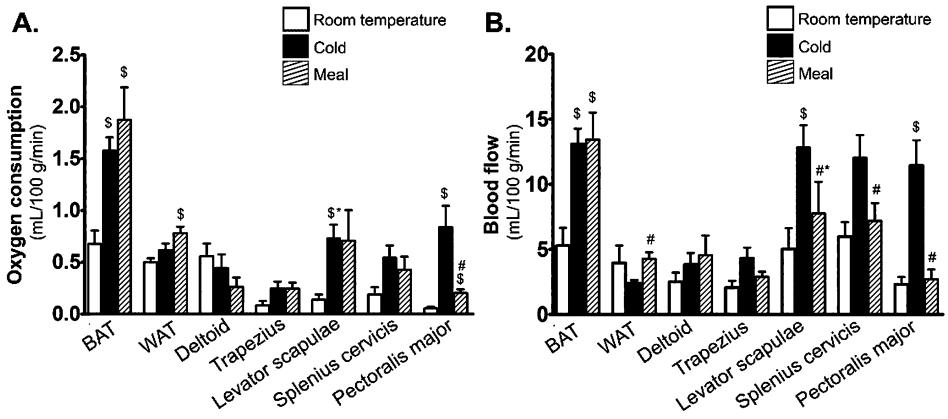

Figure 9. Oxygen consumption and blood flow of BAT and additional tissues

A: Oxygen consumption. **B**: Blood flow.

Results are presented as mean ± SEM.

$ significantly different from room temperature measurement ($p < 0.05$)

significant difference between cold and meal measurements ($p < 0.05$)

* Wilcoxon-rank sum test

Modified from U Din et al. 2018 (**II**)

5.2 BAT-specific energy expenditure and BAT mass (I – II)

Based on the oxygen consumption measurements of BAT the energy expenditure specific to BAT was estimated: at fasting room temperature, cold and after meal ingestion. The estimated BAT-specific energy expenditure in healthy human adults as follows,

- Fasting room temperature: 5 ± 2 (range: 3 – 10) kcal/day/100g of BAT
- Mild cold stress: 11 ± 4 (range: 4 – 19) kcal/day/100g of BAT
- Postprandial state: 13 ± 8 (range: 3 – 28) kcal/day/100g of BAT

In these study subjects, the BAT mass within the cervico-thoracic region was estimated to be 113 ± 66 grams (range: 2 – 275 grams). Thus, the individual BAT-specific energy expenditure values are dependent on the individual BAT masses, which was found to be quite variable in these study subjects.

5.3 Circulatory NEFA as an oxidative substrate for BAT (I – II)

The contribution of circulatory NEFA as an oxidative substrate was accessed by comparing the energy equivalent value of BAT circulatory NEFA uptake following complete oxidation and BAT-specific energy expenditure (estimated from oxygen consumption). At room temperature the circulatory NEFA uptake had an energy equivalent of almost 47 percent of the total energy produced by BAT. During the cold stress the energy equivalent of NEFA was almost 35 percent, while in the postprandial state the mean energy equivalent of circulatory NEFA uptake was 6 percent of the total energy produced by BAT. Figure 10 shows the comparison of BAT-specific total energy expenditure and contribution of circulatory NEFA to this total energy expenditure at room temperature, during cold stress and in a postprandial state.

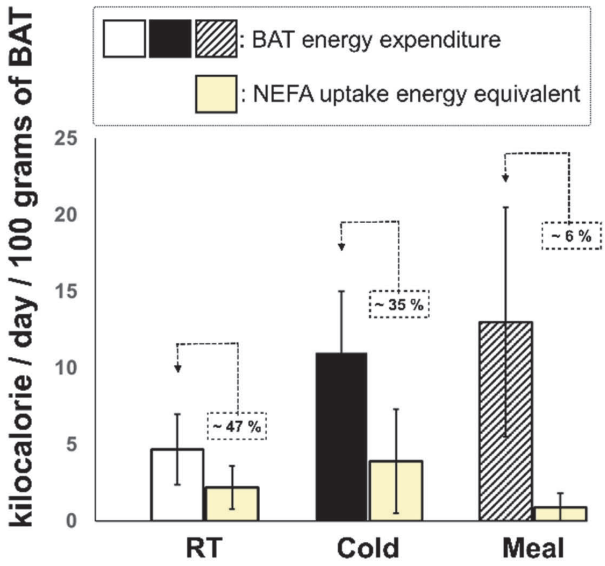

Figure 10. The comparison of BAT-specific energy expenditure and energy equivalent of NEFA uptake by BAT at room temperature (RT), during cold stress and after the ingestion of a carbohydrate dominant meal.
The results in this graph are presented as mean ± SD.

5.4 Cold and meal-induced whole-body thermogenesis (I – II)

The mild cold stress and the ingestion of a carbohydrate dominant mixed meal increased the whole-body energy expenditure. Different fuel-types for energy metabolism were used in the mild cold stress compared to after the mixed meal ingestion, as evident from different respiratory quotients. During the mild cold stress, similar to fasting room temperature conditions, whole-body fat oxidation was significantly higher than the whole-body carbohydrate oxidation. After the meal ingestion, whole body carbohydrate oxidation was significantly higher than whole-body fat oxidation. The subjects with high active BAT (High-BAT) displayed high energy expenditure per unit of fat free whole-body mass in a postprandial state, compared to the subjects with low active BAT (Low-BAT). This difference in energy expenditure was specifically due to the differences in postprandial whole-body carbohydrate oxidation, while no differences were observed in postprandial whole-body fat oxidation. The results of the whole-body energy expenditure have been shown in Figure 11.

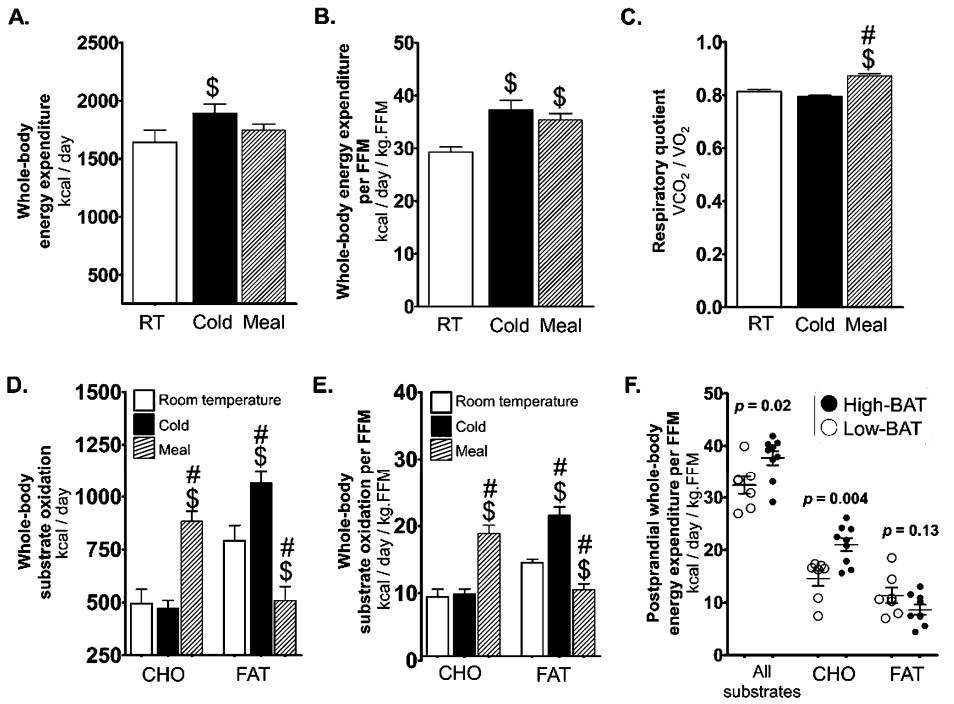

Figure 11. Whole-body energy expenditure measurements at room temperature, during cold stimulation and after meal ingestion

A: Whole-body energy expenditure. **B:** Rate of whole body energy expenditure per kilogram of fat free mass. **C:** Respiratory quotient. **D:** Whole-body substrate oxidation. **E:** Rate of whole body substrate oxidation per kilogram of fat free mass. **F:** Rate of postprandial whole body substrate oxidation per kilogram of fat free mass in High-BAT and Low-BAT study subjects.

$ significantly different from room temperature measurement ($p < 0.05$)

significant difference between cold and meal measurements ($p < 0.05$)

Modified from U Din et al. 2018 **(II)**

5.5 Circulatory hormones and metabolites at RT, cold, and after a meal (I – II)

The blood samples taken during the scanning sessions showed the response of the circulatory hormones and metabolites at RT, during cold stress and after the ingestion of a meal. These responses can be seen in Figure 12.

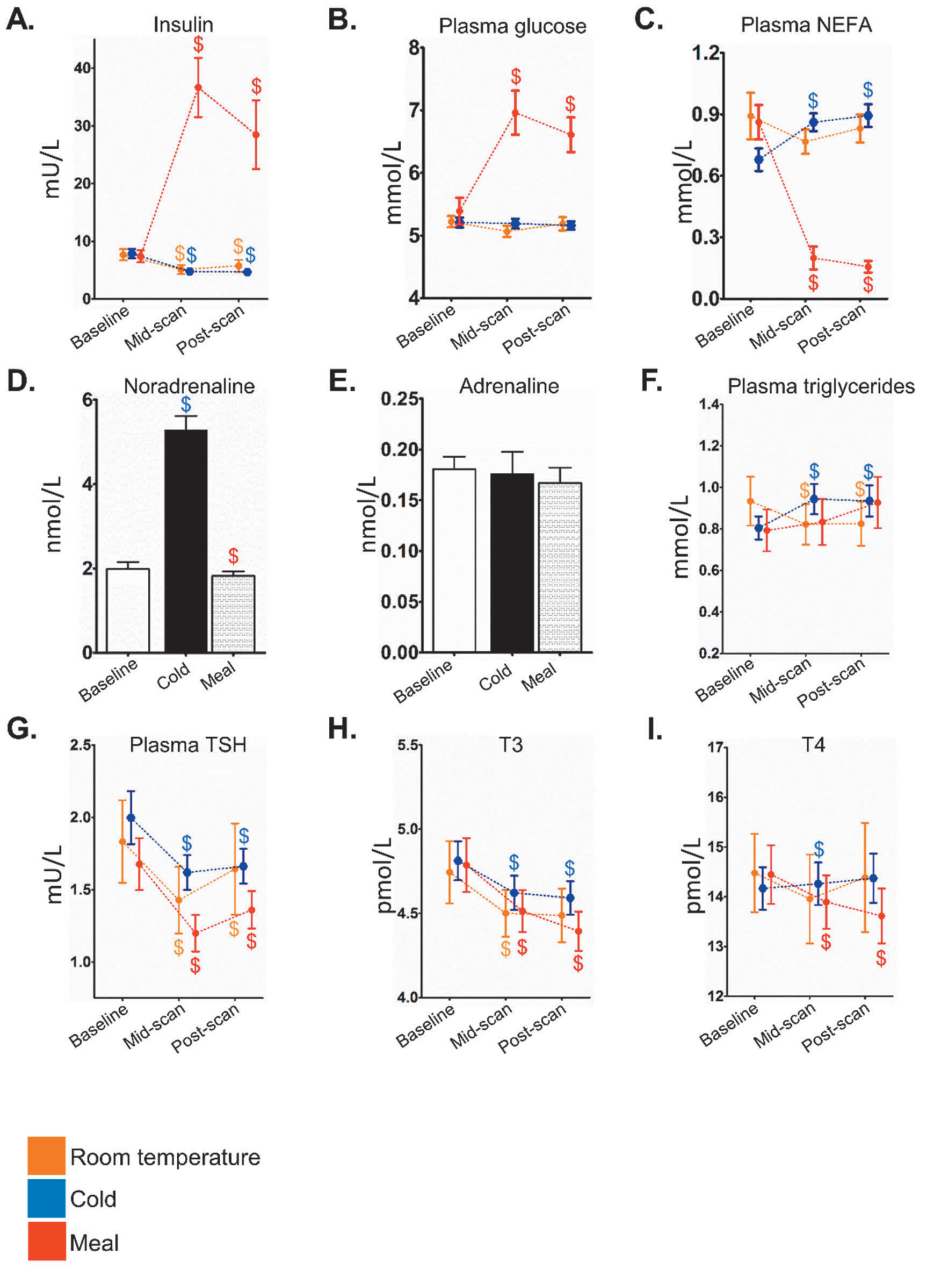

Figure 12. Concentration of circulatory hormones and metabolites at room temperature, during cold stimulation, and after meal ingestion

A: Insulin. **B:** Plasma glucose. **C:** Plasma NEFA. **D:** Noradrenaline. **E:** Adrenaline. **F:** Plasma triglycerides. **G:** Plasma TSH. **H:** T3. **I:** T4.

$ significantly different from baseline measurement ($p < 0.05$)

Modified from U Din et al. 2018 (**II**)

5.6 Comparison of high-BAT and low-BAT study subjects (III)

The comparison between subjects with high active BAT (high-BAT) and low active BAT (low-BAT) was performed. The high-BAT group was defined as those subjects who displayed cold stimulated BAT NEFA uptake of greater than 0.7 µmol/100g/min or cold stimulated BAT glucose uptake of greater than 3.0 µmol/100g/min. The comparison between the groups has been shown in Table 3.

Table 3. The comparison of high-BAT and low-BAT study subjects

Parameter		Groups based on BAT activity			
		Low-BAT	High-BAT	*p* – value	Cohen's *d*
n		24	42	-	-
Gender		10 F / 14 M	35 F / 7 M	-	-
Age (years)		43.4 ± 7.8	36.4 ± 10.1	0.005	0.78
BMI (kg/m^2)		27.6 ± 5.4	24.2 ± 3.1	0.001	0.8
Waist (cm)		93.1 ± 18.2	82.1 ± 12.5	0.006	0.72
Weight (kg)		84.0 ± 19.1	68.6 ± 11.8	0.0001	0.99
Insulin sensitivity (M-value) (µmol/kg/min)		36.8 ± 21.2	47.1 ± 19.4	0.065	0.51
Hip circumference (cm)		102.8 ± 12.1	96.8 ± 9.1	0.03	0.57
Plasma triglycerides (mmol/L)		1.0 ± 0.7	0.9 ± 0.6	0.13*	0.15
LDL-cholesterol (mmol/L)		2.9 ± 0.7	2.5 ± 0.7	0.035	0.57
HDL-cholesterol (mmol/L)		1.5 ± 0.3	1.8 ± 0.4	0.02	0.86
BAT stored triglyceride content (^{1}H-MRS) (percent)		84.3 ± 3.4	75.6 ± 8.0	0.001	1.53
BAT blood perfusion (ml/100 g/min)	RT	5.6 ± 3.6	8.8 ± 3.9	0.02	0.85
	Cold	10.4 ± 4.2$	14.6 ± 6.3$	0.007	0.80
BAT retained arterial blood (ml/100 g)	RT	2.1 ± 1.6	2.5 ± 3.0	0.62	0.17
	Cold	3.5 ± 3.2	7.8 ± 5.5$	0.001	0.98
Whole-body energy expenditure (MJ/day)	RT	7.1 ± 1.4	5.9 ± 1.1	0.01	0.96
	Cold	7.9 ± 1.6$	7.2 ± 1.5$	0.099	0.45
Cold induced change (Δ) in whole-body energy expenditure (MJ/day)		1.3 ± 1.1	0.9 ± 1.1	0.41	0.36

Data are shown as mean ± SD
Low-BAT and high-BAT groups have been compared with independent sample Student's t-test, unless otherwise stated
* Mann-Whitney *U* test
$ Significantly different than corresponding RT measurement in a paired analysis, $p < 0.05$, paired sample Student's t-test

Modified from U Din et al. 2017 (**III**)

5.7 BAT radiodensity and underlying tissue composition (III)

The radiodensity of the BAT was found to directly correlate with the tissue retained volume of arterial blood (V_A) measured with a [^{15}O]H_2O PET tracer. It was found to be inversely related to the percentage of triglycerides stored in the brown adipose tissue depot, measured with ^{1}H-MRS. Figure 13, shows these relationships.

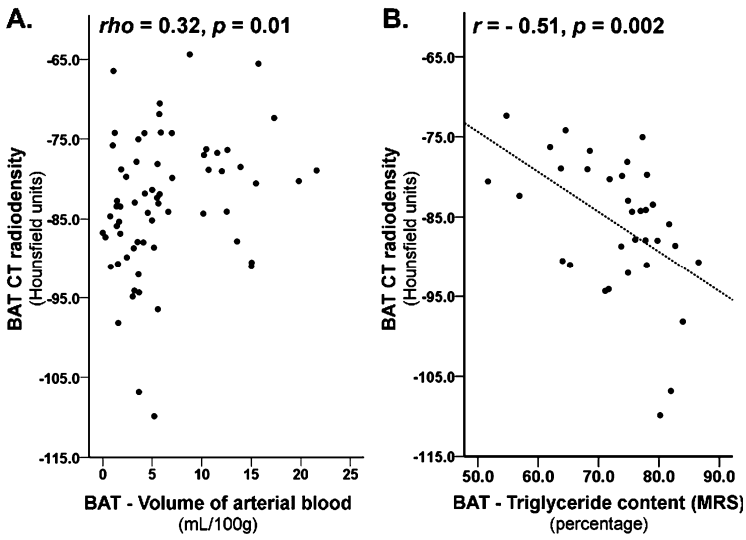

Figure 13. Relationship of CT derived BAT radiodensity and underlying tissue composition measurements.

A: Cold stimulated BAT radiodensity and volume of tissue retained arterial blood. **B:** Cold stimulated BAT radiodensity and BAT triglyceride content measured with ^{1}H-MRS.

Modified from U Din et al. 2017 (**III**)

5.8 Effect of cold stimulus and meal on BAT radiodensity (II – III)

The radiodensity of BAT was found to be effected by the cold stimulus. The cold stimulation significantly increased the radiodensity of BAT. The paired comparison of cold and meal stimulated BAT radiodensity revealed no significant difference.

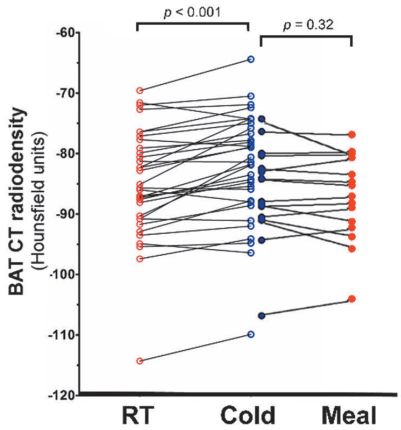

Figure 14. The effect of cold stimulation and meal ingestion on BAT radiodensity.
The cold stimulation increased the radiodensity of BAT. There was no significant difference in BAT radiodensity during cold stimulation and after the ingestion of a meal.
Modified from U Din et al. 2018 (**II**) and U Din et al. 2017 (**III**)

5.9 BAT composition and systemic metabolic health (III)

BAT radiodensity, at RT and cold, was found to be linked to the systemic metabolic health parameters. BAT radiodensity was inversely associated to obesity parameters i.e. waist circumference (Figure 15A), BMI, hip circumference. These correlations remained significant once adjusted for age in a multivariate linear regression analysis. A higher BAT radiodensity corresponded to a healthy systemic lipid profile [plasma triglyceride (Figure 15B), LDL, HDL], although these associations lost their statistical significance threshold once adjusted for BMI. BAT radiodensity, at RT and cold, was also found to be related to whole-body insulin sensitivity [M-value (Figure 15C)]. This association remained significant once adjusted separately with either BMI, waist circumference, sex or age.

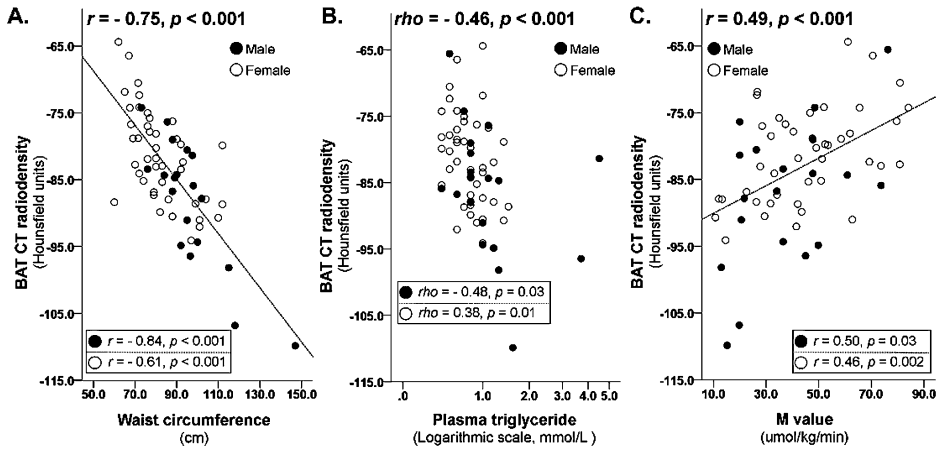

Figure 15. Relationship of CT derived BAT radiodensity and systemic metabolic health parameters.

A: BAT radiodensity and waist circumference. **B:** BAT radiodensity and plasma triglycerides. **C:** BAT radiodensity and whole body insulin sensitivity (M-value).

Modified from U Din et al. 2017 (**III**)

5.10 BAT composition and cold induced circulatory NEFA uptake (I, III)

During the cold stimulation, BAT radiodensity was found to be linked to the circulatory NEFA uptake into the BAT (Figure 16A). Moreover, it was also found that during cold stimulation the percentage of energy BAT required from the circulatory NEFA was also related to the BAT radiodensity (Figure 16B).

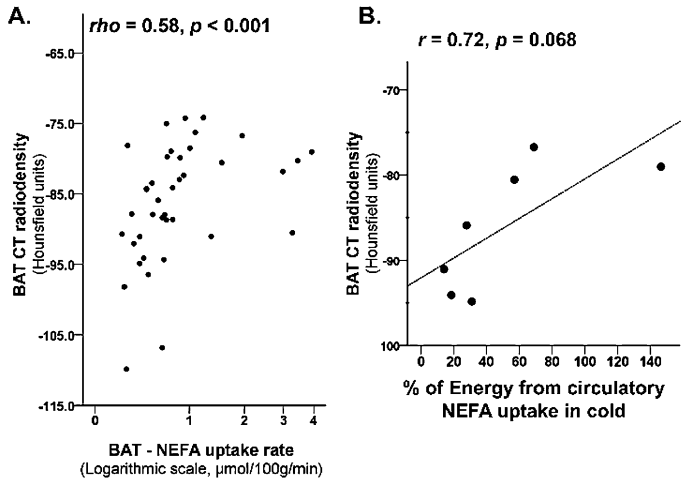

Figure 16. Relationship of CT derived BAT radiodensity and circulatory NEFA.
A: BAT radiodensity and NEFA uptake rate during cold stimulation. **B:** Contribution of circulatory NEFA towards total energy production by BAT during cold stimulation is linked to BAT composition (radiodensity). Modified from U Din et al. 2016 (**I**) and U Din et al. 2017 (**III**)

6 DISCUSSION

6.1 Oxygen consumption and substrate utilisation by BAT

In 2009, with the confirmation of the presence of functional BAT in adult humans by employing the PET imaging and biochemical analysis of human BAT biopsy specimens (Cypess et al., 2009; van Marken Lichtenbelt et al., 2009; Virtanen et al., 2009), it was speculated that activated BAT in humans has a substantial potential to contribute to energy expenditure. As discussed in section 2.2.1, the tissue-specific energy expenditure can be estimated from the measurement of tissue-specific oxygen consumption. Hence, the studies in this thesis aimed to measure the oxygen consumption of BAT using $[^{15}O]O_2$ PET imaging.

These measurements with $[^{15}O]O_2$ PET imaging revealed that the BAT in adult humans has an elevated oxygen consumption during cold stress, and as well as after the ingestion of a carbohydrate rich mixed meal. This elevated oxygen consumption likely represents an increased thermogenic state since the oxidative metabolism in BAT is linked to UCP-1 mediated heat production.

In relation to these studies and previously published evidence, the oxidative metabolism along with substrate utilisation by BAT in cold stress and postprandial state will now be discussed.

6.1.1 Cold stress

During cold stress, the activation of the sympathetic nervous system increases the circulatory catecholamine levels (Stocks et al., 2004), the noradrenaline acts on β_3-adenorecptors and after a cascade of signals (described in section 2.2.2) the mitochondrial respiration (β-oxidation, CAC, oxidative phosphorylation) increases. The increased oxygen demand by the elevated mitochondrial respiration is thus met by the increased blood perfusion to BAT, as shown in studies I – II and previous studies (Orava et al., 2011). The presence of high levels of UCP-1 in the mitochondria of the brown adipocytes diminishes the proton gradient by uncoupling the mitochondrial respiration without producing ATP, and thus the energy is dissipated in the form of heat (Cannon and

Nedergaard, 2004). The produced heat, as a result of increased mitochondrial respiration, is distributed to the rest of the body via blood circulation.

The increased thermogenesis in BAT as a result of cold stress is maintained by the continuous supply of substrates needed for thermogenic mitochondrial respiratory reactions. The substrates are provided through circulation and also via intracellular stores. Several studies report an increase in circulatory glucose uptake in BAT after acute cold exposure (Orava et al., 2011; Saito et al., 2009; Virtanen et al., 2009; Yoneshiro et al., 2011). Studies I and II provide evidence of an increased circulatory NEFA uptake in BAT during cold stress. Additionally, Study III provides an indication of the consumption of intracellular lipids in cold activated BAT (section 6.3). Despite the majority of the human BAT studies utilise [^{18}F]FDG PET imaging to study BAT metabolism, glucose has been considered as a secondary substrate for BAT (Virtanen et al., 2009); while NEFA is regarded as a main substrate (Blondin et al., 2017a; Ma and Foster, 1986); though, it can be argued based on the findings in studies I - III, and previously (Blondin et al., 2015b), that the primary choice of substrate in BAT during the cold stress is likely dependent on the cellular composition of brown adipocytes, and also the metabolic flexibility of an individual. Figure 17 summarises the oxidative and substrate metabolism of BAT during cold stress in a schematic diagram.

Interestingly, in addition to elevated oxygen consumption by BAT, in the Studies I - II, it was found that several deep muscles of the cervico-thoracic region also manifest an increased oxygen consumption in response to cold. This suggests that these muscles also play a role in cold induced thermogenesis. The exact mechanism behind this deep-muscle associated thermogenesis is unclear; it can be due to the shivering on a micro-scale level before being perceived by the individual, or it can also be due to the mitochondrial uncoupling proteins (Mollica et al., 2005; Simonyan et al., 2001; Wijers et al., 2008) and/or the sarcolipin-endoplasmic reticulum Ca^{2+}-ATPase pump interaction (Bal et al., 2012; Pant et al., 2016). Furthermore, it is also unknown whether BAT subsequent to an acute cold stimulus influences the metabolism of the muscles by the release of some ‘batokines’, or signalling molecules.

6.1.2 Postprandial state

After the ingestion of a carbohydrate rich mixed meal, the blood glucose levels rise. The increase in blood glucose stimulates the production of insulin. Insulin has an enhancing effect on the expression of GLUT-4 in BAT (Teruel et al., 1996). The increased expression of GLUT-4 in BAT stimulates the uptake of glucose from the circulation (Omatsu-Kanbe et al., 1996). Thus, the insulin induces an increased glucose uptake in BAT (Ebner et al., 1987; Klein et al., 2002; Orava et al., 2011). Insulin is also known to enhance the activity of lipoprotein lipase in BAT (Carneheim and Alexson, 1989), thus effecting the uptake of NEFA. Simultaneously, the high insulin concentration supresses lipolysis which results in suppression of circulatory NEFA. Therefore, in a postprandial state the circulatory NEFA uptake in BAT is minimal (II). While insulin may not directly activate thermogenesis in BAT (Orava et al., 2011), it may induce an increased thermogenesis by inhibiting the warm-sensitive neurons in hypothalamus, and thus effecting the BAT via central mechanism (Labbé et al., 2015; Sanchez-Alavez et al., 2010). The findings presented in Study II confirms this; thus, showing that in a postprandial state BAT has an elevated oxygen consumption (thermogenesis) and BAT likely utilise glucose as substrate for postprandial thermogenesis, as shown previously (Vosselman et al., 2013). However, the variability in thermogenesis in BAT is linked with the variation in circulatory uptake of NEFA, which most likely suggests that NEFA in BAT act as a physiological activator of UCP-1, as also indicated previously (Marette and Bukowiecki, 1991). Figure 17 illustrates the postprandial oxidative and substrate metabolism of BAT in a schematic diagram.

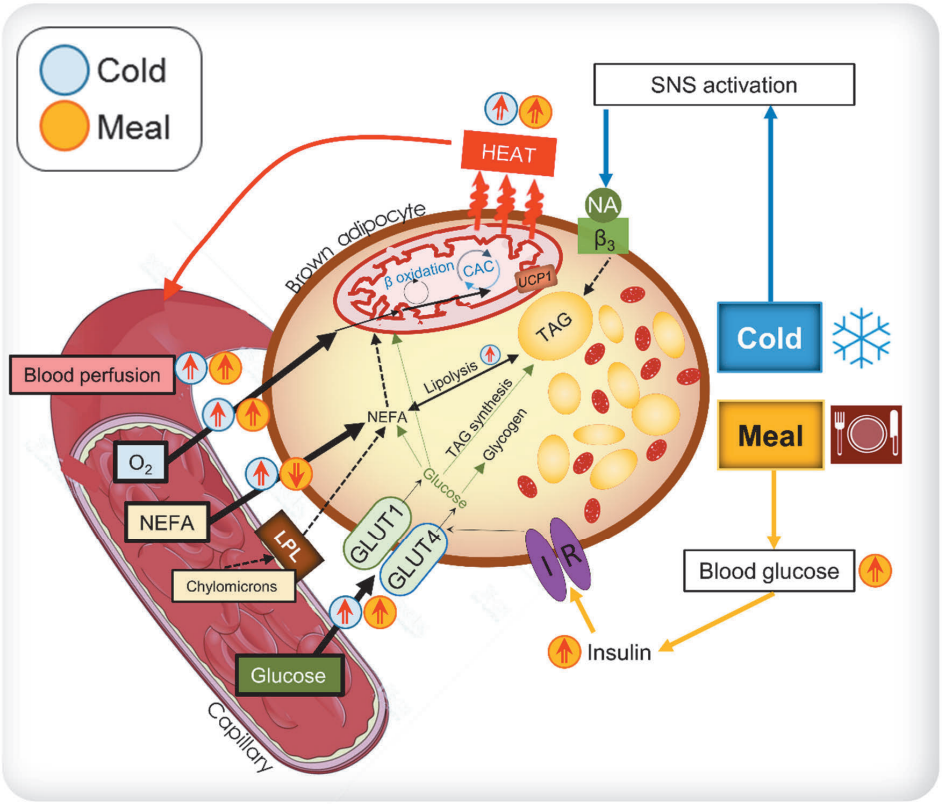

Figure 17. A schematic diagram illustrating the oxidative and substrate metabolism in a brown adipocyte during cold stress and after the ingestion of a mixed meal.

The diagram is based on the findings presented in this thesis, as well other related published literature (references are provided in the main text).

6.2 Contribution of BAT to whole-body energy metabolism

Oxygen consumption is closely related to energy expenditure; the amount of the oxygen consumption can provide an indirect estimate of the total energy expenditure of a particular tissue, organ, or an entire organism (Lusk, 1928). In a case the respiratory quotient is 1, the consumption of one litre of the oxygen yields 5 kilocalories of energy, while in a case where the respiratory quotient is 0.7, the consumption of one litre of the oxygen yields 4.7 kilocalories of energy (Leonard, 2010). Since $[^{15}O]O_2$ PET measurements do not provide the rate of

CO_2 production, the respiratory quotient therefore remains unknown. Hence, a middle value for the respiratory quotient (0.8) can be used to provide an estimate of the energy expenditure from the oxygen consumption of the tissue. The mass of the tissue also plays a significant role in determining the energy expenditure of a particular tissue or organ. The mass of the cervico-thoracic BAT is estimated by the method described in Section 4.7.6, and the corresponding results are shown in Section 5.2.

The measurements with PET-CT revealed that the energy expenditure of BAT at RT is almost 7 ± 5 kcal/day, and during the cold stress and postprandial state it can account for approximately 13 ± 7 kcal/day. This magnitude of EE signifies that BAT is a minor thermogenic tissue when compared with the daily resting energy expenditure of an average human body (1600 – 2000 kcal/day). The limited magnitude of BAT towards whole-body EE is due to the limited mass of BAT in an adult human body, despite the oxygen consumption per 100 gram of BAT is higher than the WAT and cervico-thoracic muscles. The mass of WAT and muscles constitute a major part of the adult human body, and thus they contribute more importantly to the whole-body EE. These estimates of the tissue specific energy expenditure also reveal that during cold stress, the deep muscles of the cervico-thoracic region have a significantly higher contribution (compared to BAT) to whole-body cold induced thermogenesis.

6.3 X-ray computed tomography and BAT (characterisation and metabolism)

X-ray computed tomography is a widely utilised tool, both in clinical and experimental setting, for anatomical tissue localisation in the human body (EuroStat, 2013). The utility of CT imaging to provide metabolic information has not been widely explored, particularly for BAT. Study III shows that the radiodensity of BAT is linked with the ^{1}H-MRS measured triglyceride content of BAT, and additionally [^{15}O]H_2O PET measured BAT retained volume of arterial blood volume (V_A). Thus, the CT radiodensity of BAT can be used as a marker for the underlying tissue composition, in terms of stored triglycerides and vascularity. As discussed in the section 2.1, the morphological differences in WAT and BAT are the amount of stored lipids, and tissue vascularity. Thus, the

CT imaging can be exploited to identify adipose tissue regions with less lipids and higher vascularity, a typical BAT composition.

Since BAT is considered to also rely on endogenously produced NEFA, after the lipolysis of the stored lipids, Study III examined whether the cold exposure had an effect on the CT radiodensity of BAT. The change in CT radiodensity subsequent to cold exposure likely represented the change in tissue composition, signifying a change in the amount of BAT triglyceride stores and also the amount of retained arterial blood volume. The cold exposure significantly altered the composition of BAT as reflected in the change in BAT radiodensity. This suggests that during cold stimulation BAT has either increased lipolytic activity in response to cold stimulation, or an increase in retained blood volume due to an increased perfusion, or most likely both phenomena are occurring simultaneously. The PET measurement confirmed an increase in retained blood volume in BAT in response to cold stimulation. However, the ^{1}H-MRS measurement was solitarily performed in room temperature conditions. A paired ^{1}H-MRS measurement during cold stimulation could have confirmed a decrease in stored triglycerides; however, several other studies have already confirmed this phenomenon (Blondin et al., 2017a; Gifford et al., 2016; Koskensalo et al., 2017; Lundstrom et al., 2015).

6.4 Impact of BAT on whole-body systemic metabolic health

Several studies, including Study III, have compared the metabolism of the subjects based on the metabolic activity of BAT (Baba et al., 2010; Matsushita et al., 2014; Muzik et al., 2013; Orava et al., 2011; Yoneshiro et al., 2011). It should be noticed however that most of these studies have looked into the cross-sectional data; and additionally, in these studies the ‘High-BAT’ and ‘Low-BAT’ groups are defined on the basis of the substrate uptake tracers, it can be argued that substrate uptake of the tracers does not provide complete information on whether the BAT is thermogenically active. The longitudinal studies where the recruitment or/and activation of BAT has been studied, provide the evidence that the improvement of metabolic health occurs in conjunction with the activation of BAT (Hanssen et al., 2015b, 2016; van der Lans et al., 2013). However, the precise role of BAT in improving the metabolic health in adult humans is still equivocal. Studies I - II show that BAT does have a local thermogenic role, and

can possibly combust the circulating substrates to maintain the levels of circulatory lipids and glucose within an adequate range. However, the limited thermogenic capacity, as evident from these findings, is likely not sufficient to use BAT activation as a treatment option for obesity and its related metabolic diseases, *e.g.* type II diabetes mellitus. However, the role of perpetually activated BAT for the purpose of weight management should nevertheless still not be ruled out. Additionally, the interplay of organ cross talk by the release of 'batokines' to regulate whole-body energy metabolism is still unexplored, and warrants additional studies to draw some concrete conclusions.

6.5 Limitation of the study

The present studies included only BAT in the cervico-upper thoracic region. This is because the modern day PET scanners, including the ones used in Studies I - III, have a limited FOV (15 – 20 cm). The limited FOV restricts the assessment of the whole-body, or a wider area, simultaneously. This is particularly restrictive for the scans involving ^{15}O incorporated radiotracers due to the very short half-life of the ^{15}O (122.24 sec). This limitation also restricted seeing the response of other organs in comparison to the metabolism of BAT.

The cooling protocol utilised in these studies (I – III) had the aim of delivering cold stress at a level below overt muscle tremors to the study participants, irrespective of the body adiposity. It can be argued that the present cooling protocol may have delivered a cold stress of a variable magnitude, which may have created a bias in the measurements due to the differences in cooling response of each subject. Additionally, the inclusion of an objective and quantitative approach to measure shivering (*e.g.*, electromyography) could have improved the present cooling protocol. However, presently there are no suitable non-invasive methods to detect shivering in deep muscles.

In terms of substrate utilisation, in these studies either circulatory fatty acid or glucose uptake in BAT has been measured; it would have been an optimal situation if these two parameters could be studied simultaneously in the same experimental setting. The measurement of these two substrates could possibly allow a better understanding of the substrate metabolism of BAT in different situations, particularly in the postprandial situation where the substrate uptake of NEFA is limited, and it has been speculated that the glucose is a major substrate

for meal-induced BAT thermogenesis. Since PET-CT scans involve exposure to radiation; therefore, [^{18}F]FDG and [^{18}F]FTHA scans in the same subject could not be performed, and the methodology of PET is also a constraint to measure these parameters simultaneously. In addition, the contributory role of the endogenously produced NEFAs in BAT metabolism could not be determined. There is currently no feasible method to study the rate of consumption of these endogenously produced NEFAs following intracellular lipolysis. The method utilised in Study III measuring CT radiodensity merely indicates the consumption of intracellular stores during cold stimulation. Thus, there is room for development of the methodology to study the metabolism of intracellular lipids as a source of substrate in human BAT.

Overall, despite constraints and a room for improvements in these studies, the findings presented here are genuine, and these findings lead to solid conclusions enhancing the understanding of BAT metabolism in adult humans.

7 CONCLUSIONS

- Cold stimulation increases the oxygen consumption of BAT in healthy adult humans, demonstrating an active contributory role of BAT in non-shivering thermogenesis; however, this contribution of BAT to whole-body cold-induced thermogenesis is minimal.

- The oxygen consumption of BAT in healthy adult humans after the ingestion of a carbohydrates dominant mixed meal is enhanced, suggesting a contributory role of BAT in meal-induced thermogenesis; although this contribution compared to whole-body meal-induced thermogenesis is limited.

- The x-ray computed tomography derived radiodensity measurement of BAT in healthy adult humans provides an insight into the underlying tissue composition in terms of stored triglycerides and local vascularity. In addition, the BAT stored triglycerides have an influence on BAT circulatory substrate uptake.

- The x-ray computed tomography derived radiodensity of BAT gives an insight into the systemic metabolic health of healthy adult humans; thus, suggesting a highly vascular, less triglyceride-rich BAT is a marker of superior metabolic health.

ACKNOWLEDGEMENTS

This study was carried out at the Turku PET Centre, University of Turku and Turku University Hospital. It was financially supported by the European Union, as well as grants from Academy of Finland, Diabetes Research Foundation, Finnish Cultural Foundation, Turku University Hospital, Turku University Foundation, and Doctoral programme of Clinical Research, University of Turku. I express my appreciation to Professor Juhani Knuuti, the Director of Turku PET Centre, and Professor Jaakko Hartiala and Adjunct Professor Jukka Kempainen from the Department of Clinical Physiology and Isotope Medicine for providing excellent research facilities.

I wish to express my deepest gratitude to my supervisors, Docent Kirsi Virtanen and Professor Pirjo Nuutila, who gave me the opportunity to carry out this doctoral thesis work. Over the years I have learnt a great deal of science from them. Kirsi, I deeply appreciate the level of trust and belief you have put in me. I truly admire the independence and freedom you have provided me to bring out my creativity. I am thankful for introducing me to worldwide scientific community and promoting me on several forums. Pirjo, I warmly thank you for channelling me to the right direction over the process of this doctoral work. Your guidance based on your extensive experience and knowledge has made this process easier. Thank you for teaching and always supporting me.

I am grateful to Eriika Savintaus, member of my PhD follow-up committee, for providing guidance over the years. I also wish to thank the reviewers, Professor Abdul Dulloo and Professor Esa Hohtola, for their constructive comments that helped me to improve this thesis. And I am also thankful to Professor Atso Raasmaja for accepting the role of the dissertation opponent.

I am privileged to have excellent co-authors and colleagues. Juho Raiko is deeply appreciated for his role in the studies included in this doctoral thesis, as well as his support as an excellent senior colleague. I am thankful to Teemu Saari for providing his support throughout this doctoral work. Teemu, I also admire your company in many of our trips abroad for the scientific presentations. I am deeply thankful to Minna Lahesmaa for helping me in so many levels, you are an amazing colleague and friend. I truly admire our discussions and how we have experienced the process of doctoral work side-by-side. I wish to thank my fellow researchers at Turku PET centre, Jarna Hannukainen, Kari Kalliokoski, Eleni Rebelos, Sanna Laurila, Miikka Honka, Kumail Motiani, Priyanka Motiani, Prince Dadson, Luis Edvardo, Simona Malaspina, Aino Hyypiä, and Harri Merisaari for their friendliness and help, and for keeping up the spirit.

I acknowledge Vesa Oikonen, Nobu Kudomi and Marco Bucci for providing their expertise in the issues related to PET mathematical modelling. I also wish to thank the physicists, Jarmo Teuho, Virva Saunavaara, Tuula Tolvanen, Kalle Koskensalo and Mikä Teräs for providing their crucial expertise for the physical aspects of medical images. I am grateful to Tommi Nipoinen for teaching me the processing of calorimetric data, this skill in-particular helped me immensely over the course of this doctoral work. Hannu Sipilä, Nina Savisto and Olof Solin are acknowledged for providing great radiochemistry facilities. I am thankful to Mia Koutu for taking care of practical things during the scanning sessions. I wish to thank Riitta Parkkola for providing her insight from radiological view-point. I thank Tarja Niemi and Markku Taittonen for providing their expertise in invasive BAT biopsy procedures.

I give my sincere thanks to Sauli Pirola, Timo Laitinen, Rami Mikkola and Marko Tättäläinen for providing the IT and Carimas support. For secretarial matters Mirja Jyrkinen and Lenita Saloranta are greatly acknowledged. I warmly thank Kristiina Nuutila and Eeva Raino for providing the support in the matters related to the graduate school.

I wish to express my sincere gratitude to all the volunteer subjects for their participation in the studies.

I am forever thankful to my old teachers and mentors; particularly, Najam Uddin for introducing me to the world of medical imaging. John Eriksson, for providing an excellent support during my master's degree years. Tony Shepherd, for introducing me to the Turku PET centre; and Amir Snapir for providing an insight to the world outside academia.

I am also thankful to my friends outside of workplace in Turku and beyond, Basit Butt, Farid Ahmed, Meraj Khan, Mohammad Shahnoor, Moin Khan, Umar Butt, Umar Jawa, Wajiha Bano, Zeeshan Azhar, Mari Routsalo, and Tanel Routsalo. Our excursions, cricket matches, talks and food get-togethers have always been fun.

I am very fortunate to have very close friends, Pir Shariq and Soukaina Mezgheldi. Shariq, in our long friendship we have shared so much together. It is a great pleasure to have a friend like you and I am thankful for always being there for me. Soukaina, I am deeply grateful for your support, encouragement, understanding and patience. Our conversations have brought me joy and they have made me see things more clearly and eventually make sound judgments. Our friendship has made me a better person.

I am thankful to my beloved sisters, Arooj and Adiya, and my dear brother, Hamza, for always admiring what I do, and providing excellent support as well as joyous moments in our get-togethers. I am also thankful to Arooj's husband Hassan, and the little one, Aisha for bringing the smiles.

Finally, I express my deepest gratitude to my parents, Talib Mehmood Sheikh and Malahat Sheikh, for always encouraging me to pursue my life ambitions and dreams. I am really thankful that among countless other things, you have taught me how to remain optimistic in everyday life situations, and how to always see good in people. Your suggestions about life-related practical matter have broadened my vision. And, I truly believe your prayers have been quite useful during the process of this doctoral thesis.

Turku, Finland – April, 2018

Mueez u Din

REFERENCES

Aherne, W., and Hull, D. (1966). Brown adipose tissue and heat production in the newborn infant. *The Journal of Pathology and Bacteriology* 91, 223–234.

Ahmadi, N., Hajsadeghi, F., Conneely, M., Mingos, M., Arora, R., Budoff, M., and Ebrahimi, R. (2013). Accurate detection of metabolically active "brown" and "white" adipose tissues with computed tomography. *Academic Radiology* 20, 1443–1447.

Aquila, H., Link, T.A., and Klingenberg, M. (1985). The uncoupling protein from brown fat mitochondria is related to the mitochondrial ADP/ATP carrier. Analysis of sequence homologies and of folding of the protein in the membrane. *The EMBO Journal* 4, 2369–2376.

Atit, R., Sgaier, S.K., Mohamed, O.A., Taketo, M.M., Dufort, D., Joyner, A.L., Niswander, L., and Conlon, R.A. (2006). B-Catenin Activation Is Necessary and Sufficient To Specify the Dorsal Dermal Fate in the Mouse. *Developmental Biology* 296, 164–176.

Baba, S., Jacene, H.A., Engles, J.M., Honda, H., and Wahl, R.L. (2010). CT Hounsfield Units of Brown Adipose Tissue Increase with Activation: Preclinical and Clinical Studies. *Journal of Nuclear Medicine* 51, 246–250.

Bal, N.C., Maurya, S.K., Sopariwala, D.H., Sahoo, S.K., Gupta, S.C., Shaikh, S.A., Pant, M., Rowland, L.A., Goonasekera, S.A., Molkentin, J.D., Periasamy, M., Molkentin, J.D., and Periasamy, M. (2012). Sarcolipin is a newly identified regulator of muscle-based thermogenesis in mammals. *Nature Medicine* 18, 1575–1579.

Barquissau, V., Beuzelin, D., Pisani, D.F., Beranger, G.E., Mairal, A., Montagner, A., Roussel, B., Tavernier, G., Marques, M.-A., Moro, C., Guillou, H., Amri, E.-Z., and Langin, D. (2016). White-to-brite conversion in human adipocytes promotes metabolic reprogramming towards fatty acid anabolic and catabolic pathways. *Molecular Metabolism* 5, 352–365.

Bartness, T.J., Vaughan, C.H., and Song, C.K. (2010). Sympathetic and sensory innervation of brown adipose tissue. *International Journal of Obesity* 34, S36–S42.

Berbée, J.F.P., Boon, M.R., Khedoe, P.P.S.J., Bartelt, A., Schlein, C., Worthmann, A., Kooijman, S., Hoeke, G., Mol, I.M., John, C., Jung, C., Vazirpanah, N., Brouwers, L.P.J., Gordts, P.L.S.M., Esko, J.D., Hiemstra, P.S., Havekes, L.M., Scheja, L., Heeren, J., and Rensen, P.C.N. (2015). Brown fat activation reduces hypercholesterolaemia and protects from atherosclerosis development. *Nature Communications* 6, 6356.

Bjorndal, B., Burri, L., Staalesen, V., Skorve, J., and Berge, R.K. (2011). Different adipose depots: their role in the development of metabolic syndrome and mitochondrial response to hypolipidemic agents. *Journal of Obesity.* 2011, 490650-.

Blondin, D.P., Labbé, S.M., Tingelstad, H.C., Noll, C., Kunach,

M., Phoenix, S., Guérin, B., Turcotte, É.E., Carpentier, A.C., Richard, D., and Haman, F. (2014). Increased brown adipose tissue oxidative capacity in cold-acclimated humans. *Journal of Clinical Endocrinology and Metabolism* 99, E438–E446.

Blondin, D.P., Labbé, S.M., Phoenix, S., Guérin, B., Turcotte, É.E., Richard, D., Carpentier, A.C., and Haman, F. (2015a). Contributions of white and brown adipose tissues and skeletal muscles to acute cold-induced metabolic responses in healthy men. *The Journal of Physiology* 593, 701–714.

Blondin, D.P., Labbé, S.M., Noll, C., Kunach, M., Phoenix, S., Guérin, B., Turcotte, É.E., Haman, F., Richard, D., and Carpentier, A.C. (2015b). Selective Impairment of Glucose but Not Fatty Acid or Oxidative Metabolism in Brown Adipose Tissue of Subjects With Type 2 Diabetes. *Diabetes* 64, 2388–2397.

Blondin, D.P., Frisch, F., Phoenix, S., Guérin, B., Turcotte, É.E., Haman, F., Richard, D., and Carpentier, A.C. (2017a). Inhibition of Intracellular Triglyceride Lipolysis Suppresses Cold-Induced Brown Adipose Tissue Metabolism and Increases Shivering in Humans. *Cell Metabolism* 25, 438–447.

Blondin, D.P., Tingelstad, H.C., Noll, C., Frisch, F., Phoenix, S., Guérin, B., Turcotte, É.E., Richard, D., Haman, F., and Carpentier, A.C. (2017b). Dietary fatty acid metabolism of brown adipose tissue in cold-acclimated men. *Nature Communications* 8, 14146.

Bordicchia, M., Liu, D., Amri, E.-Z., Ailhaud, G., Dessì-Fulgheri, P., Zhang, C., Takahashi, N., Sarzani, R., and Collins, S. (2012). Cardiac natriuretic peptides act via p38 MAPK to induce the brown fat thermogenic program in mouse and human adipocytes. *The Journal of Clinical Investigation* 122, 1022–1036.

Borum, P.R. (1991). Carnitine and lipid metabolism. *Boletin de La Asociacion Medica de Puerto Rico* 83, 134–135.

Bouillaud, F., Weissenbach, J., and Ricquier, D. (1986). Complete cDNA-derived amino acid sequence of rat brown fat uncoupling protein. *The Journal of Biological Chemistry* 261, 1487–1490.

Bourová, L., Pesanová, Z., Novotný, J., Bengtsson, T., and Svoboda, P. (2000). Differentiation of cultured brown adipocytes is associated with a selective increase in the short variant of g(s)alpha protein. Evidence for higher functional activity of g(s)alphaS. *Molecular and Cellular Endocrinology* 167, 23–31.

Broeders, E.P.M., Nascimento, E.B.M., Havekes, B., Brans, B., Roumans, K.H.M., Tailleux, A., Schaart, G., Kouach, M., Charton, J., Deprez, B., Bouvy, N.D., Mottaghy, F., Staels, B., van Marken Lichtenbelt, W.D., and Schrauwen, P. (2015). The Bile Acid Chenodeoxycholic Acid Increases Human Brown Adipose Tissue Activity. *Cell Metabolism* 22, 418–426.

Buxton, D.B., Schwaiger, M., Nguyen, A., Phelps, M.E., and Schelbert, H.R. (1988). Radiolabeled acetate as a tracer of myocardial tricarboxylic acid cycle flux. *Circulation Research* 63, 628–634.

Cannon, B., and Nedergaard, J. (2004). Brown Adipose Tissue: Function and Physiological Significance. *Physiological Reviews* 84, 277–359.

Carneheim, C.M., and Alexson, S.E.

(1989). Refeeding and insulin increase lipoprotein lipase activity in rat brown adipose tissue. *The American Journal of Physiology* 256, E645-50.

Chaudhry, A., and Granneman, J.G. (1999). Differential regulation of functional responses by beta-adrenergic receptor subtypes in brown adipocytes. *The American Journal of Physiology* 277, R147-53.

Chen, Y.-C., Cypess, A.M., Chen, Y.-C., Palmer, M., Kolodny, G., Kahn, C.R., and Kwong, K.K. (2013). Measurement of Human Brown Adipose Tissue Volume and Activity Using Anatomic MR Imaging and Functional MR Imaging. *Journal of Nuclear Medicine* 54, 1584–1587.

Cherry, S.R., and Dahlbom, M. (2006). PET: Physics, Instrumentation, and Scanners. In PET, Michael E. Phelps, ed. (New York, NY: Springer New York), pp. 1–117.

Chondronikola, M., Porter, C., Malagaris, I., Nella, A.A., and Sidossis, L.S. (2017). Brown adipose tissue is associated with systemic concentrations of peptides secreted from the gastrointestinal system and involved in appetite regulation. *European Journal of Endocrinology* 177, 33–40.

Ciarelli, M.J., Goldstein, S.A., Kuhn, J.L., Cody, D.D., and Brown, M.B. (1991). Evaluation of orthogonal mechanical properties and density of human trabecular bone from the major metaphyseal regions with materials testing and computed tomography. *Journal of Orthopaedic Research* 9, 674–682.

Cinti, S. (2005). The adipose organ. *Prostaglandins Leukotrienes and Essential Fatty Acids* 73, 9–15.

Cinti, S. (2006). The role of brown adipose tissue in human obesity. *Nutrition, Metabolism and Cardiovascular Diseases* 16, 569–574.

Cinti, S. (2009). Transdifferentiation properties of adipocytes in the adipose organ. *AJP: Endocrinology and Metabolism* 297, E977–E986.

Cinti S (2012). The adipose organ at a glance. *Disease Models & Mechanisms* 5, 588–594.

Clockaerts, S., Bastiaansen-Jenniskens, Y.M., Runhaar, J., Van Osch, G.J.V.M., Van Offel, J.F., Verhaar, J.A.N., De Clerck, L.S., and Somville, J. (2010). The infrapatellar fat pad should be considered as an active osteoarthritic joint tissue: a narrative review. *Osteoarthritis and Cartilage* 18, 876–882.

Cohade, C., Osman, M., Pannu, H.K., and Wahl, R.L. (2003). Uptake in supraclavicular area fat ("USA-Fat"): description on 18F-FDG PET/CT. *Journal of Nuclear Medicine* 44, 170–176.

Collins, S., and Bordicchia, M. (2013). Heart hormones fueling a fire in fat. *Adipocyte* 2, 104–108.

Crichton, P.G., Lee, Y., and Kunji, E.R.S. (2017). The molecular features of uncoupling protein 1 support a conventional mitochondrial carrier-like mechanism. *Biochimie* 134, 35–50.

Cypess, A.M., and Kahn, C.R. (2010). Brown fat as a therapy for obesity and diabetes. *Current Opinion in Endocrinology, Diabetes and Obesity* 17, 143–149.

Cypess, A.M., Lehman, S., Williams, G., Tal, I., Rodman, D., Goldfine, A.B., Kuo, F.C., Palmer, E.L., Tseng, Y.-H., Doria, A., Kolodny, G.M., and Kahn, C.R. (2009). Identification and Importance of Brown Adipose Tissue in Adult

Humans. *New England Journal of Medicine* 360, 1509–1517.

DeFronzo, R. a, Tobin, J.D., and Andres, R. (1979). Glucose clamp technique: a method for quantifying insulin secretion and resistance. *The American Journal of Physiology* 237, E214–E223.

Divakaruni, A.S., Humphrey, D.M., and Brand, M.D. (2012). Fatty Acids Change the Conformation of Uncoupling Protein 1 (UCP1). *Journal of Biological Chemistry* 287, 36845–36853.

Ebner, S., Burnol, A.F., Ferre, P., de Saintaurin, M.A., and Girard, J. (1987). Effects of insulin and norepinephrine on glucose transport and metabolism in rat brown adipocytes. Potentiation by insulin of norepinephrine-induced glucose oxidation. *European Journal of Biochemistry* 170, 469–474.

Ellis, P.D. (2009). Effect size calculator.

Enerbäck, S. (2009). The Origins of Brown Adipose Tissue. *New England Journal of Medicine* 360, 2021–2023.

EuroStat (2013). Healthcare resource statistics - technical resources and medical technology. http://ec.europa.eu/eurostat/statistics-explained/.

Fares, A. (2013). Winter cardiovascular diseases phenomenon. *North American Journal of Medical Sciences* 5, 266–279.

Fedorenko, A., Lishko, P. V, and Kirichok, Y. (2012). Mechanism of fatty-acid-dependent UCP1 uncoupling in brown fat mitochondria. *Cell* 151, 400–413.

Ferrannini, E. (1988). The theoretical bases of indirect calorimetry: A review. *Metabolism* 37, 287–301.

Fisher, F.M., Kleiner, S., Douris, N., Fox, E.C., Mepani, R.J., Verdeguer, F., Wu, J., Kharitonenkov, A., Flier, J.S., Maratos-Flier, E., and Spiegelman, B.M. (2012). FGF21 regulates PGC-1α and browning of white adipose tissues in adaptive thermogenesis. *Genes & Development* 26, 271–281.

Florea, V.G., and Cohn, J.N. (2014). The autonomic nervous system and heart failure. *Circulation Research* 114, 1815–1826.

Friedewald, W.T., Levy, R.I., and Fredrickson, D.S. (1972). Estimation of the concentration of low-density lipoprotein cholesterol in plasma, without use of the preparative ultracentrifuge. *Clinical Chemistry* 18, 499–502.

Gerngroß, C., Schretter, J., Klingenspor, M., Schwaiger, M., and Fromme, T. (2017). Active Brown Fat During ^{18}F-FDG PET/CT Imaging Defines a Patient Group with Characteristic Traits and an Increased Probability of Brown Fat Redetection. *Journal of Nuclear Medicine* 58, 1104–1110.

Gesta, S., Tseng, Y.H., and Kahn, C.R. (2007). Developmental origin of fat: tracking obesity to its source. *Cell* 131, 242–256.

Gifford, A., Towse, T.F., Walker, R.C., Avison, M.J., and Welch, E.B. (2016). Characterizing active and inactive brown adipose tissue in adult humans using PET-CT and MR imaging. *American Journal of Physiology - Endocrinology And Metabolism* 311, E95–E104.

Glick, Z., Teague, R., and Bray, G. (1981). Brown adipose tissue: thermic response increased by a single low protein, high carbohydrate meal. *Science* 213, 1125–1127.

Goldberg, I.J., Eckel, R.H., and Abumrad, N.A. (2009). Regulation of fatty acid uptake into tissues:

lipoprotein lipase- and CD36-mediated pathways: Fig. 1. *Journal of Lipid Research* 50, S86–S90.

Hamacher, K., Coenen, H.H., and Stöcklin, G. (1986). Efficient stereospecific synthesis of no-carrier-added 2-[18F]-fluoro-2-deoxy-D-glucose using aminopolyether supported nucleophilic substitution. *Journal of Nuclear Medicine* 27, 235–238.

Hanssen, M.J.W., Broeders, E., Samms, R.J., Vosselman, M.J., van der Lans, A.A.J.J., Cheng, C.C., Adams, A.C., van Marken Lichtenbelt, W.D., and Schrauwen, P. (2015a). Serum FGF21 levels are associated with brown adipose tissue activity in humans. *Scientific Reports* 5, 10275.

Hanssen, M.J.W., Hoeks, J., Brans, B., van der Lans, A.A.J.J., Schaart, G., van den Driessche, J.J., Jörgensen, J.A., Boekschoten, M. V, Hesselink, M.K.C., Havekes, B., Kersten, S., Mottaghy, F.M., van Marken Lichtenbelt, W.D., and Schrauwen, P. (2015b). Short-term cold acclimation improves insulin sensitivity in patients with type 2 diabetes mellitus. *Nature Medicine* 21, 863–865.

Hanssen, M.J.W., Van Der Lans, A.A.J.J., Brans, B., Hoeks, J., Jardon, K.M.C., Schaart, G., Mottaghy, F.M., Schrauwen, P., and Van Marken Lichtenbelt, W.D. (2016). Short-term cold acclimation recruits brown adipose tissue in obese humans. *Diabetes* 65, 1179–1189.

Hausberger, F.X., and Widelitz, M.M. (1963). Distribution of labeled erythrocytes in adipose tissue and muscle in the rat. *The American Journal of Physiology* 204, 649–652.

Heaton, J.M. (1972). The distribution of brown adipose tissue in the human. *Journal of Anatomy* 112, 35–39.

Hoeke, G., Kooijman, S., Boon, M.R., Rensen, P.C.N., and Berbeé, J.F.P. (2016). Role of Brown Fat in Lipoprotein Metabolism and Atherosclerosis. *Circulation Research* 118, 173–182.

Holstila, M., Virtanen, K.A., Grönroos, T.J., Laine, J., Lepomäki, V., Saunavaara, J., Lisinen, I., Komu, M., Hannukainen, J.C., Nuutila, P., Parkkola, R., and Borra, R.J.H. (2013). Measurement of brown adipose tissue mass using a novel dual-echo magnetic resonance imaging approach: A validation study. *Metabolism: Clinical and Experimental* 62, 1189–1198.

Holstila, M., Pesola, M., Saari, T., Koskensalo, K., Raiko, J., Borra, R.J.H., Nuutila, P., Parkkola, R., and Virtanen, K.A. (2017). MR signal-fat-fraction analysis and T2* weighted imaging measure BAT reliably on humans without cold exposure. *Metabolism* 70, 23–30.

Hondares, E., Rosell, M., Gonzalez, F.J., Giralt, M., Iglesias, R., and Villarroya, F. (2010). Hepatic FGF21 Expression Is Induced at Birth via PPARα in Response to Milk Intake and Contributes to Thermogenic Activation of Neonatal Brown Fat. *Cell Metabolism* 11, 206–212.

Hori, Y., Hirano, Y., Koshino, K., Moriguchi, T., Iguchi, S., Yamamoto, A., Enmi, J., Kawashima, H., Zeniya, T., Morita, N., Nakagawara, J., Casey, M.E., and Iida, H. (2014). Validity of using a 3-dimensional PET scanner during inhalation of (15)O-labeled oxygen for quantitative assessment of regional metabolic rate of oxygen in man. *Physics in Medicine and Biology* 59, 5593–

5609.

Hu, H.H., Chung, S.A., Nayak, K., Jackson, H.A., and Gilsanz, V. (2010). Differential computed tomographic attenuation of metabolically active and inactive adipose tissues: preliminary findings. *Journal of Computer Assisted Tomography* 35, 65–71.

Iacobellis, G., Corradi, D., and Sharma, A.M. (2005). Epicardial adipose tissue: anatomic, biomolecular and clinical relationships with the heart. *Nature Clinical Practice. Cardiovascular Medicine* 2, 536–543.

Iida, H., Jones, T., and Miura, S. (1993). Modeling approach to eliminate the need to separate arterial plasma in oxygen-15 inhalation positron emission tomography. *Journal of Nuclear Medicine : Official Publication, Society of Nuclear Medicine* 34, 1333–1340.

Ilankovan, V., and Soames, J. V (1995). Morphometric analysis of orbital, buccal and subcutaneous fats: their potential in the treatment of enophthalmos. *The British Journal of Oral & Maxillofacial Surgery* 33, 40–42.

Inokuma, K., Ogura-Okamatsu, Y., Toda, C., Kimura, K., Yamashita, H., and Saito, M. (2005). Uncoupling protein 1 is necessary for norepinephrine-induced glucose utilization in brown adipose tissue. *Diabetes* 54, 1385–1391.

Ishibashi, J., and Seale, P. (2010). Beige can be slimming. *Science* 328, 1113–1114.

Jespersen, N.Z., Larsen, T.J., Peijs, L., Daugaard, S., Homøe, P., Loft, A., de Jong, J., Mathur, N., Cannon, B., Nedergaard, J., Pedersen, B.K., Møller, K., and Scheele, C. (2013). A Classical Brown Adipose Tissue mRNA Signature Partly Overlaps with Brite in the Supraclavicular Region of Adult Humans. *Cell Metabolism* 17, 798–805.

Jezek, P., and Garlid, K.D. (1998). Mammalian mitochondrial uncoupling proteins. *The International Journal of Biochemistry & Cell Biology* 30, 1163–1168.

Keyes, J.W. (1995). SUV: standard uptake or silly useless value? *Journal of Nuclear Medicine* 36, 1836–1839.

Klein, J., Fasshauer, M., Klein, H.H., Benito, M., and Kahn, C.R. (2002). Novel adipocyte lines from brown fat: a model system for the study of differentiation, energy metabolism, and insulin action. *BioEssays : News and Reviews in Molecular, Cellular and Developmental Biology* 24, 382–388.

Klein, L.J., Visser, F.C., Knaapen, P., Peters, J.H., Teule, G.J.J., Visser, C.A., and Lammertsma, A.A. (2001). Carbon-11 acetate as a tracer of myocardial oxygen consumption. *European Journal of Nuclear Medicine* 28, 651–668.

Klingenspor, M. (2003). Cold-induced recruitment of brown adipose tissue thermogenesis. *Experimental Physiology* 88, 141–148.

Koksharova, E., Ustyuzhanin, D., Philippov, Y., Mayorov, A., Shestakova, M., Shariya, M., Ternovoy, S., and Dedov, I. (2017). The Relationship Between Brown Adipose Tissue Content in Supraclavicular Fat Depots and Insulin Sensitivity in Patients with Type 2 Diabetes Mellitus and Prediabetes. *Diabetes Technology & Therapeutics* 19, 96–102.

Konrad, D., Bilan, P.J., Nawaz, Z., Sweeney, G., Niu, W., Liu, Z., Antonescu, C.N., Rudich, A., and Klip, A. (2002). Need for GLUT4

activation to reach maximum effect of insulin-mediated glucose uptake in brown adipocytes isolated from GLUT4myc-expressing mice. *Diabetes* 51, 2719–2726.

Kooijman, S., van den Heuvel, J.K., and Rensen, P.C.N. (2015). Neuronal Control of Brown Fat Activity. *Trends in Endocrinology & Metabolism* 26, 657–668.

Koskensalo, K., Raiko, J., Saari, T., Saunavaara, V., Eskola, O., Nuutila, P., Saunavaara, J., Parkkola, R., and Virtanen, K.A. (2017). Human brown adipose tissue temperature and fat fraction are related to its metabolic activity. *Journal of Clinical Endocrinology and Metabolism* 102, 1200–1207.

Kozak, L.P. (2010). Brown Fat and the Myth of Diet-Induced Thermogenesis. *Cell Metabolism* 11, 263–267.

Kramarova, T. V., Shabalina, I.G., Andersson, U., Westerberg, R., Carlberg, I., Houstek, J., Nedergaard, J., and Cannon, B. (2007). Mitochondrial ATP synthase levels in brown adipose tissue are governed by the c-Fo subunit P1 isoform. *The FASEB Journal* 22, 55–63.

Krebs, H.A. (1948). The tricarboxylic acid cycle. *Harvey Lectures* Series 44, 165–199.

Krintel, C., Mörgelin, M., Logan, D.T., and Holm, C. (2009). Phosphorylation of hormone-sensitive lipase by protein kinase A in vitro promotes an increase in its hydrophobic surface area. *The FEBS Journal* 276, 4752–4762.

Kudomi, N., Hirano, Y., Koshino, K., Hayashi, T., Watabe, H., Fukushima, K., Moriwaki, H., Teramoto, N., Iihara, K., and Iida, H. (2013). Rapid Quantitative *CBF* and *CMRO* $_2$ Measurements from a Single *PET* Scan with Sequential Administration of Dual ^{15} O-Labeled Tracers. *Journal of Cerebral Blood Flow & Metabolism* 33, 440–448.

Labbé, S.M., Caron, A., Lanfray, D., Monge-Rofarello, B., Bartness, T.J., and Richard, D. (2015). Hypothalamic control of brown adipose tissue thermogenesis. *Frontiers in Systems Neuroscience* 9, 150.

van der Lans, A.A.J.J., Hoeks, J., Brans, B., Vijgen, G.H.E.J., Visser, M.G.W.M.G.W., Vosselman, M.J., Hansen, J., Jorgensen, J.A., Wu, J., Mottaghy, F.M., Schrauwen, P., van Marken Lichtenbelt, W.D., Jörgensen, J.A., Wu, J., Mottaghy, F.M., Schrauwen, P., and van Marken Lichtenbelt, W.D. (2013). Cold acclimation recruit human brown fat and increases nonshivering thermogenesis. *The Journal of Clinical Investigation* 123, 3395–3403.

Laplante, M., Festuccia, W.T., Soucy, G., Blanchard, P.-G., Renaud, A., Berger, J.P., Olivecrona, G., and Deshaies, Y. (2008). Tissue-specific postprandial clearance is the major determinant of PPAR -induced triglyceride lowering in the rat. *AJP: Regulatory, Integrative and Comparative Physiology* 296, R57–R66.

Lean, M.E.J., and James, W.P.T. (1983). Uncoupling protein in human brown adipose tissue mitochondria. Isolation and detection by specific antiserum. *FEBS Letters* 163, 235–240.

Lee, P., Smith, S., Linderman, J., Courville, A.B., Brychta, R.J., Dieckmann, W., Werner, C.D., Chen, K.Y., and Celi, F.S. (2014). Temperature-acclimated brown adipose tissue modulates insulin sensitivity in humans. *Diabetes* 63, 3686–3698.

Leonard, W.R. (2010). Measuring human energy expenditure and metabolic function: basic principles and methods. *Journal of Anthropological Sciences = Rivista Di Antropologia : JASS / Istituto Italiano Di Antropologia* 88, 221–230.

Lidell, M.E., Betz, M.J., Leinhard, O.D., Heglind, M., Elander, L., Slawik, M., Mussack, T., Nilsson, D., Romu, T., Nuutila, P., Virtanen, K.A., Beuschlein, F., Persson, A., Borga, M., and Enerbäck, S. (2013). Evidence for two types of brown adipose tissue in humans. *Nature Medicine* 19, 631–634.

Lindberg, O., de Pierre, J., Rylander, E., and Afzelius, B.A. (1967). Studies of the mitochondrial energy-transfer system of brown adipose tissue. *Journal of Cell Biology* 34, 293–310.

Lobo, S., Wiczer, B.M., Smith, A.J., Hall, A.M., and Bernlohr, D.A. (2007). Fatty acid metabolism in adipocytes: functional analysis of fatty acid transport proteins 1 and 4. *Journal of Lipid Research* 48, 609–620.

Lundstrom, E., Strand, R., Johansson, L., Bergsten, P., Ahlstrom, H., and Kullberg, J. (2015). Magnetic resonance imaging cooling-reheating protocol indicates decreased fat fraction via lipid consumption in suspected brown adipose tissue. *PLoS.One.* 10, e0126705-.

Lusk, G. (1928). The elements of the science of nutrition (Philadelphia: Saunders Company).

Ma, S.W.Y., and Foster, D.O. (1986). Uptake of glucose and release of fatty acids and glycerol by rat brown adipose tissue *in vivo*. *Canadian Journal of Physiology and Pharmacology* 64, 609–614.

Marette, A., and Bukowiecki, L.J. (1991). Noradrenaline stimulates glucose transport in rat brown adipocytes by activating thermogenesis. Evidence that fatty acid activation of mitochondrial respiration enhances glucose transport. *The Biochemical Journal* 277 (Pt 1), 119–124.

van Marken Lichtenbelt, W.D., Vanhommerig, J.W., Smulders, N.M., Drossaerts, J.M.A.F.L., Kemerink, G.J., Bouvy, N.D., Schrauwen, P., and Teule, G.J.J. (2009). Cold-Activated Brown Adipose Tissue in Healthy Men. *New England Journal of Medicine* 360, 1500–1508.

Matsushita, M., Yoneshiro, T., Aita, S., Kameya, T., Sugie, H., and Saito, M. (2014). Impact of brown adipose tissue on body fatness and glucose metabolism in healthy humans. *International Journal of Obesity* 38, 812–817.

Mattu, A., Brady, W.J., and Perron, A.D. (2002). Electrocardiographic manifestations of hypothermia. *The American Journal of Emergency Medicine* 20, 314–326.

Mazoyer, B.M., Huesman, R.H., Budinger, T.F., and Knittel, B.L. (1986). Dynamic PET data analysis. *Journal of Computer Assisted Tomography* 10, 645–653.

McBroom, R.J., Hayes, W.C., Edwards, W.T., Goldberg, R.P., and White, A.A. (1985). Prediction of vertebral body compressive fracture using quantitative computed tomography. *The Journal of Bone and Joint Surgery. American Volume* 67, 1206–1214.

McCallister, A., Zhang, L., Burant, A., Katz, L., and Branca, R.T. (2017). A pilot study on the correlation between fat fraction

values and glucose uptake values in supraclavicular fat by simultaneous PET/MRI. *Magnetic Resonance in Medicine* 78, 1922–1932.

McKnight, G.S., Cummings, D.E., Amieux, P.S., Sikorski, M.A., Brandon, E.P., Planas, J. V, Motamed, K., and Idzerda, R.L. (1998). Cyclic AMP, PKA, and the physiological regulation of adiposity. *Recent Progress in Hormone Research* 53, 139-59-1.

Meriläinen, P.T. (1987). Metabolic monitor. *International Journal of Clinical Monitoring and Computing* 4, 167–177.

Mintun, M. a, Raichle, M.E., Martin, W.R., and Herscovitch, P. (1984). Brain oxygen utilization measured with O-15 radiotracers and positron emission tomography. *Journal of Nuclear Medicine* 25, 177–187.

Mitchell, P. (1966). Chemiosmotic coupling in oxidative and photosynthetic phosphorylation. *Biological Reviews of the Cambridge Philosophical Society* 41, 445–502.

Mitchell, P., and Moyle, J. (1967). Chemiosmotic hypothesis of oxidative phosphorylation. *Nature* 213, 137–139.

Mollica, M.P., Lionetti, L., Crescenzo, R., Tasso, R., Barletta, A., Liverini, G., and Iossa, S. (2005). Cold exposure differently influences mitochondrial energy efficiency in rat liver and skeletal muscle. *FEBS Letters* 579, 1978–1982.

Moreira, F.A., and Crippa, J.A.S. (2009). The psychiatric side-effects of rimonabant. *Revista Brasileira de Psiquiatria* 31, 145–153.

Moura, M.A.F., Festuccia, W.T.L., Kawashita, N.H., Garófalo, M.A.R., Brito, S.R.C., Kettelhut, I.C., and Migliorini, R.H. (2005). Brown adipose tissue glyceroneogenesis is activated in rats exposed to cold. *Pflugers Archiv European Journal of Physiology* 449, 463–469.

Muzi, M., O'Sullivan, F., Mankoff, D.A., Doot, R.K., Pierce, L.A., Kurland, B.F., Linden, H.M., and Kinahan, P.E. (2012). Quantitative assessment of dynamic PET imaging data in cancer imaging. *Magnetic Resonance Imaging* 30, 1203–1215.

Muzik, O., Mangner, T.J., and Granneman, J.G. (2012). Assessment of oxidative metabolism in brown fat using PET imaging. *Front Endocrinol.(Lausanne)* 3, 15-.

Muzik, O., Mangner, T.J., Leonard, W.R., Kumar, A., Janisse, J., and Granneman, J.G. (2013). 15O PET Measurement of Blood Flow and Oxygen Consumption in Cold-Activated Human Brown Fat. *Journal of Nuclear Medicine* 54, 523–531.

Nedergaard, J., and Cannon, B. (2013). UCP1 mRNA does not produce heat. *Biochimica et Biophysica Acta - Molecular and Cell Biology of Lipids* 1831, 943–949.

Nilsson, N.O., Strålfors, P., Fredrikson, G., and Belfrage, P. (1980). Regulation of adipose tissue lipolysis: effects of noradrenaline and insulin on phosphorylation of hormone-sensitive lipase and on lipolysis in intact rat adipocytes. *FEBS Letters* 111, 125–130.

Nuutila, P., Peltoniemi, P., Oikonen, V., Larmola, K., Kemppainen, J., Takala, T., Sipilä, H., Oksanen, A., Ruotsalainen, U., Bolli, G.B., and Yki-järvinen, H. (2000). Enhanced Stimulation of Glucose Uptake by Insulin Increases Exercise-Stimulated Glucose Uptake in. *Diabetes* 49, 1084.

Ohta, S., Meyer, E., Thompson, C.J., and Gjedde, A. (1992). Oxygen

Consumption of the Living Human Brain Measured after a Single Inhalation of Positron Emitting Oxygen. *Journal of Cerebral Blood Flow & Metabolism* 12, 179–192.

Oikonen V., Nuutila P., Sipilä H., Tolvanen T., Peltoniemi P., Ruotsalainen U. (1998). Quantification of oxygen consumption in skeletal muscle with PET and oxygen-15 bolus. *European Journal of Nuclear Medicine* 25, 1151-.

Omatsu-Kanbe, M., Zarnowski, M.J., and Cushman, S.W. (1996). Hormonal regulation of glucose transport in a brown adipose cell preparation isolated from rats that shows a large response to insulin. *The Biochemical Journal* 315 (Pt 1), 25–31.

Orava, J., Nuutila, P., Lidell, M.E., Oikonen, V., Noponen, T., Viljanen, T., Scheinin, M., Taittonen, M., Niemi, T., Enerbäck, S., and Virtanen, K.A. (2011). Different metabolic responses of human brown adipose tissue to activation by cold and insulin. *Cell Metabolism* 14, 272–279.

Orava, J., Nuutila, P., Noponen, T., Parkkola, R., Viljanen, T., Enerbäck, S., Rissanen, A., Pietiläinen, K.H., and Virtanen, K.A. (2013). Blunted metabolic responses to cold and insulin stimulation in brown adipose tissue of obese humans. *Obesity* 21, 2279–2287.

Ouellet, V., Labbé, S.M., Blondin, D.P., Phoenix, S., Guérin, B., Haman, F., Turcotte, E.E., Richard, D., and Carpentier, A.C. (2012). Brown adipose tissue oxidative metabolism contributes to energy expenditure during acute cold exposure in humans. *Journal of Clinical Investigation* 122, 545–552.

Pant, M., Bal, N.C., and Periasamy, M. (2016). Sarcolipin: A Key Thermogenic and Metabolic Regulator in Skeletal Muscle. *Trends in Endocrinology & Metabolism* 27, 881–892.

Patel, T.B., Du, Z., Pierre, S., Cartin, L., and Scholich, K. (2001). Molecular biological approaches to unravel adenylyl cyclase signaling and function. *Gene* 269, 13–25.

Patlak, C.S., and Blasberg, R.G. (1985). Graphical Evaluation of Blood-to-Brain Transfer Constants from Multiple-Time Uptake Data. Generalizations. *Journal of Cerebral Blood Flow & Metabolism* 5, 584–590.

Peltoniemi, P., Lönnroth, P., Laine, H., Oikonen, V., Tolvanen, T., Grönroos, T., Strindberg, L., Knuuti, J., and Nuutila, P. (2000). Lumped constant for [(18)F]fluorodeoxyglucose in skeletal muscles of obese and nonobese humans. *American Journal of Physiology. Endocrinology and Metabolism* 279, E1122-30.

Petrovic, N., Walden, T.B., Shabalina, I.G., Timmons, J.A., Cannon, B., and Nedergaard, J. (2010). Chronic peroxisome proliferator-activated receptor γ (PPARγ) activation of epididymally derived white adipocyte cultures reveals a population of thermogenically competent, UCP1-containing adipocytes molecularly distinct from classic brown adipocytes. *Journal of Biological Chemistry* 285, 7153–7164.

Phelps, M.E. (2000). Positron emission tomography provides molecular imaging of biological processes. *Proceedings of the National Academy of Sciences of the United States of America* 97, 9226–9233.

Raiko, J., Holstila, M., Virtanen,

K.A., Orava, J., Saunavaara, V., Niemi, T., Laine, J., Taittonen, M., Borra, R.J.H., Nuutila, P., and Parkkola, R. (2015). Brown adipose tissue triglyceride content is associated with decreased insulin sensitivity, independently of age and obesity. *Diabetes, Obesity and Metabolism* 17, 516–519.

Reshef, L., Olswang, Y., Cassuto, H., Blum, B., Croniger, C.M., Kalhan, S.C., Tilghman, S.M., and Hanson, R.W. (2003). Glyceroneogenesis and the triglyceride/fatty acid cycle. *The Journal of Biological Chemistry* 278, 30413–30416.

Rothwell, N.J., and Stock, M.J. (1979). A role for brown adipose tissue in diet-induced thermogenesis. *Nature* 281, 31–35.

Sacks, H., and Symonds, M.E. (2013). Anatomical locations of human brown adipose tissue: Functional relevance and implications in obesity and type 2 diabetes. *Diabetes* 62, 1783–1790.

Saha, G.B. (2010). Basics of PET Imaging (New York, NY: Springer New York).

Saito, M., Okamatsu-Ogura, Y., Matsushita, M., Watanabe, K., Yoneshiro, T., Nio-Kobayashi, J., Iwanaga, T., Miyagawa, M., Kameya, T., Nakada, K., Kawai, Y., and Tsujisaki, M. (2009). High incidence of metabolically active brown adipose tissue in healthy adult humans: Effects of cold exposure and adiposity. *Diabetes* 58, 1526–1531.

Sanchez-Alavez, M., Tabarean, I. V., Osborn, O., Mitsukawa, K., Schaefer, J., Dubins, J., Holmberg, K.H., Klein, I., Klaus, J., Gomez, L.F., Kolb, H., Secrest, J., Jochems, J., Myashiro, K., Buckley, P., Hadcock, J.R., Eberwine, J., Conti, B., and Bartfai, T. (2010). Insulin Causes Hyperthermia by Direct Inhibition of Warm-Sensitive Neurons. *Diabetes* 59, 43–50.

Sanei, M., Davarpanah, A., Jafari, H., Sanei, B., Tabatabie, S., Bigdelian, H., and Hashemi, S. (2015). Distribution of mediastinal ectopic thymic tissue in patients without thymic disease. *Advanced Biomedical Research* 4, 18.

Schlett, C.L., Massaro, J.M., Lehman, S.J., Bamberg, F., O'Donnell, C.J., Fox, C.S., and Hoffmann, U. (2009). Novel measurements of periaortic adipose tissue in comparison to anthropometric measures of obesity, and abdominal adipose tissue. *International Journal of Obesity (2005)* 33, 226–232.

Seale, P., Bjork, B., Yang, W., Kajimura, S., Chin, S., Kuang, S., Scimè, A., Devarakonda, S., Conroe, H.M., Erdjument-Bromage, H., Tempst, P., Rudnicki, M.A., Beier, D.R., and Spiegelman, B.M. (2008). PRDM16 controls a brown fat/skeletal muscle switch. *Nature* 454, 961–967.

Shabalina, I.G., Jacobsson, A., Cannon, B., and Nedergaard, J. (2004). Native UCP1 Displays Simple Competitive Kinetics between the Regulators Purine Nucleotides and Fatty Acids. *Journal of Biological Chemistry* 279, 38236–38248.

Shao, X., Yang, W., Shao, X., Qiu, C., Wang, X., and Wang, Y. (2016). The role of active brown adipose tissue (aBAT) in lipid metabolism in healthy Chinese adults. *Lipids in Health and Disease* 15, 138.

Sharp, L.Z., Shinoda, K., Ohno, H., Scheel, D.W., Tomoda, E., Ruiz, L., Hu, H., Wang, L., Pavlova, Z., Gilsanz, V., and Kajimura, S.

(2012). Human BAT possesses molecular signatures that resemble beige/brite cells. *PLoS One.* 7, e49452-.

Simonyan, R.A., Jimenez, M., Ceddia, R.B., Giacobino, J.P., Muzzin, P., and Skulachev, V.P. (2001). Cold-induced changes in the energy coupling and the UCP3 level in rodent skeletal muscles. *Biochimica et Biophysica Acta - Bioenergetics* 1505, 271–279.

Singhal, V., Maffazioli, G.D., Ackerman, K.E., Lee, H., Elia, E.F., Woolley, R., Kolodny, G., Cypess, A.M., and Misra, M. (2016). Effect of Chronic Athletic Activity on Brown Fat in Young Women. *PLoS One* 11, e0156353.

Slater, E.C. (1953). Mechanism of Phosphorylation in the Respiratory Chain. *Nature* 172, 975–978.

Smith, R.E. (1964). Thermoregulatory and Adaptive Behavior of Brown Adipose Tissue. *Science (New York, N.Y.)* 146, 1686–1689.

Stocks, J., Taylor, N., Tipton, M., and Greenleaf, J. (2004). Human physiological responses to cold exposure. *Aviation Space and Environmental Medicine* 75, 444–457.

Strijckmans, K., Vandecasteele, C., and Sambre, J. (1985). Production and quality control of 15O2 and C15O2 for medical use. *The International Journal Of Applied Radiation And Isotopes* 36, 279–283.

Takx, R.A.P., Ishai, A., Truong, Q.A., MacNabb, M.H., Scherrer-Crosbie, M., and Tawakol, A. (2016). Supraclavicular Brown Adipose Tissue 18F-FDG Uptake and Cardiovascular Disease. *Journal of Nuclear Medicine* 57, 1221–1225.

Teruel, T., Valverde, A.M., Benito, M., and Lorenzo, M. (1996). Insulin-like growth factor I and insulin induce adipogenic-related gene expression in fetal brown adipocyte primary cultures. *The Biochemical Journal* 319 (Pt 2), 627–632.

U Din, M. (2013). Differentiation of Metabolically Distinct Areas within Head and Neck Region using Dynamic 18F-FDG Positron Emission Tomography Imaging. *University of Turku*.

Vallerand, A.L., Zamecnik, J., Jones, P.J., and Jacobs, I. (1999). Cold stress increases lipolysis, FFA Ra and TG/FFA cycling in humans. *Aviation, Space, and Environmental Medicine* 70, 42–50.

Vergnes, L., Chin, R., Young, S.G., and Reue, K. (2011). Heart-type fatty acid-binding protein is essential for efficient brown adipose tissue fatty acid oxidation and cold tolerance. *The Journal of Biological Chemistry* 286, 380–390.

Villarroya, F., and Vidal-Puig, A. (2013). Beyond the sympathetic tone: The new brown fat activators. *Cell Metabolism* 17, 638–643.

Virtanen, K.A., Peltoniemi, P., Marjamäki, P., Asola, M., Strindberg, L., Parkkola, R., Huupponen, R., Knuuti, J., Lönnroth, P., and Nuutila, P. (2001). Human adipose tissue glucose uptake determined using [18F]-fluoro-deoxy-glucose ([18F]FDG) and PET in combination with microdialysis. *Diabetologia* 44, 2171–2179.

Virtanen, K.A., Lidell, M.E., Orava, J., Heglind, M., Westergren, R., Niemi, T., Taittonen, M., Laine, J., Savisto, N.-J., Enerbäck, S., and Nuutila, P. (2009). Functional Brown Adipose Tissue in Healthy Adults. *New England Journal of Medicine* 360, 1518–1525.

Vosselman, M.J., Brans, B., Van Der

Lans, A.A.J.J., Wierts, R., Van Baak, M.A., Mottaghy, F.M., Schrauwen, P., and Van Marken Lichtenbelt, W.D. (2013). Brown adipose tissue activity after a high-calorie meal in humans. *American Journal of Clinical Nutrition* 98, 57–64.

Walden, T.B., Hansen, I.R., Timmons, J.A., Cannon, B., and Nedergaard, J. (2012). Recruited vs. nonrecruited molecular signatures of brown, "brite," and white adipose tissues. *AJP: Endocrinology and Metabolism* 302, E19–E31.

Watanabe, M., Houten, S.M., Mataki, C., Christoffolete, M.A., Kim, B.W., Sato, H., Messaddeq, N., Harney, J.W., Ezaki, O., Kodama, T., Schoonjans, K., Bianco, A.C., and Auwerx, J. (2006). Bile acids induce energy expenditure by promoting intracellular thyroid hormone activation. *Nature* 439, 484–489.

Weir, J.B. de V. (1949). New methods for calculating metabolic rate with special reference to protein metabolism. *The Journal of Physiology* 109, 1–9.

Wienhard, K., Pawlik, G., Herholz, K., Wagner, R., and Heiss, W.-D. (1985). Estimation of Local Cerebral Glucose Utilization by Positron Emission Tomography of [^{18} F]2-Fluoro-2-Deoxy-D-Glucose: A Critical Appraisal of Optimization Procedures. *Journal of Cerebral Blood Flow & Metabolism* 5, 115–125.

Wijers, S.L., Schrauwen, P., Saris, W.H., and van Marken Lichtenbelt, W.D. (2008). Human skeletal muscle mitochondrial uncoupling is associated with cold induced adaptive thermogenesis. *PLoS.One.* 3, e1777-.

Wu, J., Boström, P., Sparks, L.M., Ye, L., Choi, J.H., Giang, A.H., Khandekar, M., Virtanen, K.A., Nuutila, P., Schaart, G., Huang, K., Tu, H., Van Marken Lichtenbelt, W.D., Hoeks, J., Enerbäck, S., Schrauwen, P., and Spiegelman, B.M. (2012). Beige adipocytes are a distinct type of thermogenic fat cell in mouse and human. *Cell* 150, 366–376.

Wu, Q., Kazantzis, M., Doege, H., Ortegon, A.M., Tsang, B., Falcon, A., and Stahl, A. (2006). Fatty Acid Transport Protein 1 Is Required for Nonshivering Thermogenesis in Brown Adipose Tissue. *Diabetes* 55, 3229–3237.

Wu, W., Shi, F., Liu, D., Ceddia, R.P., Gaffin, R., Wei, W., Fang, H., Lewandowski, E.D., and Collins, S. (2017). Enhancing natriuretic peptide signaling in adipose tissue, but not in muscle, protects against diet-induced obesity and insulin resistance. *Science Signaling* 10, eaam6870.

Yoneshiro, T., Aita, S., Matsushita, M., Kameya, T., Nakada, K., Kawai, Y., and Saito, M. (2011). Brown Adipose Tissue, Whole-Body Energy Expenditure, and Thermogenesis in Healthy Adult Men. *Obesity* 19, 13–16.

Young, J.B., Saville, E., Rothwell, N.J., Stock, M.J., and Landsberg, L. (1982). Effect of diet and cold exposure on norepinephrine turnover in brown adipose tissue of the rat. *The Journal of Clinical Investigation* 69, 1061–1071.

Zakaria, E., and Shafrir, E. (1967). Yellow bone marrow as adipose tissue. *Proceedings of the Society for Experimental Biology and Medicine. Society for Experimental Biology and Medicine (New York, N.Y.)* 124, 1265–1268.

Zimmermann, R., Strauss, J.G., Haemmerle, G., Schoiswohl, G.,

Birner-Gruenberger, R., Riederer, M., Lass, A., Neuberger, G., Eisenhaber, F., Hermetter, A., and Zechner, R. (2004). Fat Mobilization in Adipose Tissue Is Promoted by Adipose Triglyceride Lipase. *Science* 306, 1383–1386.

Zweig, M.H., and Campbell, G. (1993). Receiver-operating characteristic (ROC) plots: a fundamental evaluation tool in clinical medicine. *Clinical Chemistry* 39, 561–577.

Annales Universitatis Turkuensis

Turun yliopisto
University of Turku

ISBN 978-951-29-7219-7 (PRINT)
ISBN 978-951-29-7220-3 (PDF)
ISSN 0355-9483 (Print) | ISSN 2343-3213 (Online)

Painosalama Oy, Turku, Finland 2018